5-2019

Characterization of Hydride Vapor Phase Epitaxy Grown GaN Substrates for Future III-Nitride Growth

Alaa Ahmad Kawagy
University of Arkansas, Fayetteville

Characterization of Hydride Vapor Phase Epitaxy Grown GaN Substrates for Future III-Nitride Growth

A thesis submitted in partial fulfillment
of the requirements for the degree of
Master of Science in Microelectronics-Photonics

by

Alaa Kawagy
University of Jazan
Bachelor of Science in Physics, 2011

May 2019
University of Arkansas

This thesis is approved for recommendation to the Graduate Council.

Morgan Ware, Ph.D.
Thesis Director

Zhong Chen, Ph.D.
Committee Member

Cynthia Sides, Ph.D.
Committee Member

Rick Wise, Ph.D.
Ex-Officio Member

The following signatories attest that all software used in this thesis was legally licensed for use by Alaa Kawagy for research purposes and publication.

Ms. Alaa Kawagy, Student	Dr. Morgan Ware, Thesis Director

This thesis was submitted to http://www.turnitin.com for plagiarism review by the TurnItIn company's software. The signatories have examined the report on this thesis that was returned by TurnItIn and attest that, in their opinion, the items highlighted by the software are incidental to common usage and are not plagiarized material.

Dr. Rick Wise, Program Director	Dr. Morgan Ware, Thesis Director

Abstract

The aim of this research is to investigate and characterize the quality of commercially obtained gallium nitride (GaN) on sapphire substrates that have been grown using hydride vapor phase epitaxy (HVPE). GaN substrates are the best choice for optoelectronic applications because of their physical and electrical properties. Even though HVPE GaN substrates are available at low-cost and create the opportunities for growth and production, these substrates suffer from large macro-scale defects on the surface of the substrate.

In this research, four GaN on sapphire substrates were investigated in order to characterize the surface defects and, subsequently, understand their influence on homoepitaxial GaN growth. Two substrates were unintentionally doped (UID) GaN on sapphire, and the other two were semi-insulating (SI) GaN on sapphire which were doped with iron (Fe) in order to compensate the background doping inherent in GaN. Several characterization techniques were performed. Atomic force microscopy, scanning electron microscopy, and optical microscopy were performed to characterize the surface morphology. X-ray diffraction, cathodoluminescence, transmission measurements, and optical transmission electron microscopy were applied to study the bulk structural and optical properties.

The investigation of the surface of GaN substrates exposed various defects that are associated with defects in the structure such as dislocations, as well as vacancies and point defects. The UID GaN substrates suffered from hexagonal V-shape pits with pits densities of approximately 10^7 and 10^8 cm^{-2}, whereas, the SI GaN substrates exhibited much larger macro-scale pits with areal densities of about 10^2 cm^{-2}. X-ray diffraction results were deconvoluted in order to characterize the screw and mixed (edge and screw) dislocation densities for the studied substrates. The UID substrates exhibited screw dislocation densities of 10^7 and 10^8 cm^{-2} and

mixed dislocation densities of 10^9 and 10^{10} cm^{-2}. The SI substrates, however, exhibit generally lower densities of dislocations of 10^9 and 10^8 cm^{-2} for screw and mixed, respectively. Cathodoluminescence measurements demonstrated interesting results for the UID and SI substrates with energies of 4 and 3.5 eV, respectively. The transmission measurements for the UID substrates showed that the bandgap energy was 3.39 eV.

Acknowledgements

First of all, my deep gratitude to the God who gave me the passion to achieve my ambitions and made me look always forward. He made me always optimistic for the better and confident about my ability and what I can do.

My great gratitude to my advisor, Dr. Morgan Ware, who accepted me in his great research group. He is such an amazing advisor who helps and supports his students, and he is very patient with them. He taught me a lot about GaN and semiconductor materials during our discussions. I would like to thank him for providing all materials that I needed in my research and for making it easy to go through. If I did not understand something, I usually asked him, and he explained to me very clearly and guided me in the right direction. This thesis would not be complete without his support, advice, and encouragement.

I would like to thank every person in my research group. I would like to thank Pijush Ghosh who helped me from the beginning of my research and training in the labs. I would like to thank him for GaN growth that he did for my research. I would like to thank Alaa Alnami who supported me all the time. I would like to thank Manal Aldawsari for helping me in optical transmission measurements. I would like to thank Mirsaeid Sarollahi who helped and taught me about PL measurements. I would like to thank Reem Alhelais to helped me in cutting the samples.

I would like to thank Najla Alnami who supported me in my research. She introduced me to Dr. Ware when I asked to join his group. She always helped me when I discussed with her about semiconductors and physics.

I would like to thank Mohammed Alavijeh who usually supported me when I worked in AFM lab. He helped me to get better results.

I would like to thank Andrian Kuchuk for x-ray diffraction measurements. Also, I would like to thank Dr. Mourad Benamara and Qigeng Yan for CL and TEM measurements.

I am thankful to the director of the Microelectronic-Photonics, Dr. Rick Wise, for his guidance of such an incredible department. He always guides us from the first day in our journey to the last day. He helped me a lot by explaining the rules and providing the information that I needed to graduate. He supported me and encouraged me during my studying. Also, I would like to thank Renee Jones-Hearon who assisted me to do all documents on time.

I would like to thank my parents, Amnah and Ahmed, who support me always. I would like to thank them to allow me to travel and achieve my ambitions. I thank them for my education and my encouragement to study since I was a child. They supported me in hard times and contacted me every day to ask about me and my progress. Also, I would like to thank my brother, Hassan, and sister, Nassim, who asked about me and gave me some suggestions to pass through all the hardness.

I would like to thank my husband, Alhussain, who supported me and helped me during my graduate study. He helped me a lot during my graduating time to take care of my children, especially my daughter who is two months old. He tried to offer the best environment at home for me, so I could work and did a lot of work. I would like to thank my son, Aseel, and daughter, Nora, for their understanding of my situation. My son helped me to take care of his sister and even he sometimes cooked for me when I missed some meals.

Dedication

I dedicate this thesis to my parents, Amnah Anami and Ahmed Khawaji, my husband, Alhussain Alnami, my children, Aseel and Nora, my brother, Hassan, and my sister, Nassim, who continuedly supported me.

Table of Contents

List of Figures

List of Tables

Chapter 1: Introduction and Background

1.1 Introduction

Gallium Nitride (GaN) is a semiconductor material from that has desirable physical properties such as wide bandgap energy, high saturation velocity, and large breakdown field. GaN is used in different applications such as ultraviolet (UV) blue-green emitters, power switches, optoelectronics, electronics, and detectors (Figure 1) [1]. Heteroepitaxial approaches have been relied on for commercial realization of these applications. These heteroepitaxial approaches are employed on different substrates such as sapphire and silicon.

Even though many applications have significant efficiency, they are limited by GaN's structural quality. Native GaN has not been well established yet, and alternatives, which include a few micrometers of GaN grown epitaxially on another substrate such as sapphire, suffer from lattice mismatch, chemical incompatibility, and thermal expansion coefficient mismatch, which leads to high densities of defects and dislocations [2].

The efficiency of many devices is limited because of the structural and electronic defects in GaN. These defects have a negative impact on the lifetime of devices which utilize GaN materials. The defects in GaN have been studied for more than two decades. However, some of the formation mechanisms of these defects need to be more characterized and completely understood. GaN films are grown on foreign substrates such as sapphire and silicon [3]. The properties of sapphire (Al_2O_3) make it a good alternative substrate for GaN because of its stability at high temperature as well as its native high structural quality which can be obtained at relatively low prices [4],[5],[6]. Even though sapphire is a good alternative substrate for GaN, the lattice mismatch between sapphire and GaN is large which can induce more defects in the

GaN structure and surface. This lattice mismatch between GaN and sapphire can form structural defects and strain[7], [8].

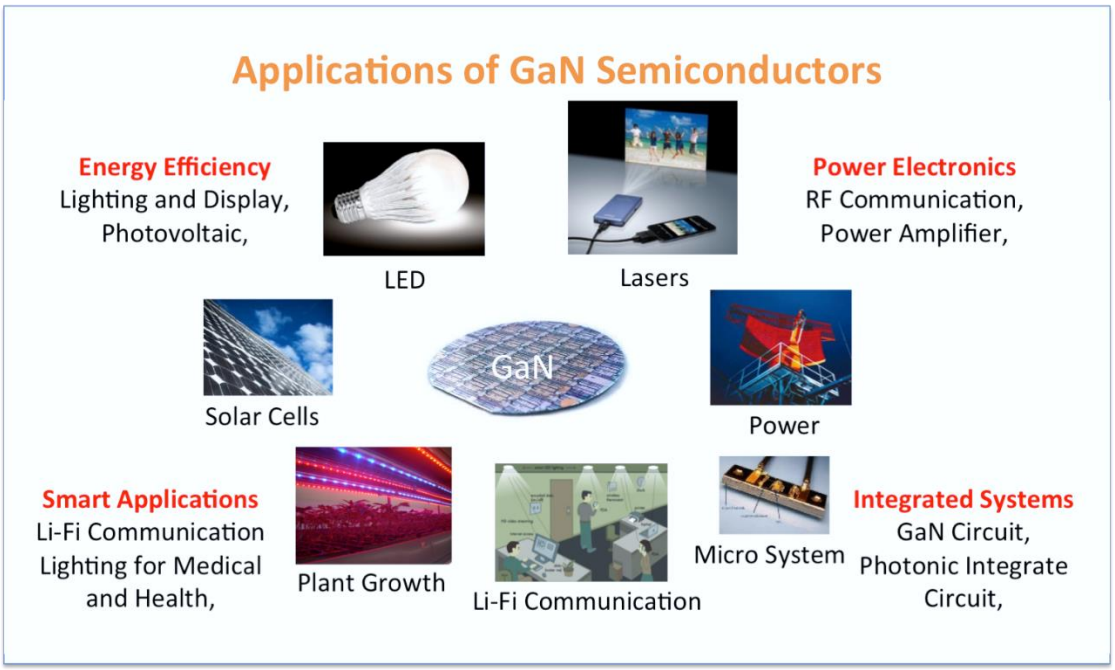

Figure 1. Some of GaN applications [1].

Although the industry is working on developing GaN using several methods of growth, it is still not possible to grow GaN without significant defects. One reason of trying to develop GaN wafers is the electronic industry and the growth of high power and high frequency transistors which require high structural quality. However, it is a challenge to crystallize GaN because of its very high melting point of greater than 2500 °C [9]. In addition, the nitrogen pressure needed for growth is higher than 6 GPa. Therefore, it is hard to form GaN by melting. However, there are other techniques to crystalize GaN which require lower pressure and temperature. These techniques can be from gas or solution. In this research, GaN substrates were grown by hydride vapor phase epitaxy which will be described later. These substrates were

grown by and purchased from Kyma Technologies, Raleigh, NC.

1.1.1 Objective of This Research

In this project, many types of characterization have been applied to get understanding of the GaN properties and defects. The characterization techniques were applied to four GaN substrates that were grown on sapphire. Two of these substrates were unintentionally doped GaN, and one of them was coated by titanium (Ti) on the backside. The other two substrates were semi-insulating GaN which was doped with iron (Fe) with density equals to 10^{18} cm^{-3}, and one of them had titanium. All of these GaN substrates were grown by Hydride Vapor Phase Epitaxy (HVPE).

The morphology of GaN substrates which were grown by HVPE were studied using atomic force microscope (AFM), optical microscope imaging for surface analysis, x-ray diffraction (XRD) for crystalline characterization, photoluminescence measurements for studying defects by luminescence, optical transmission for identifying the band gap, scanning electron microscope (SEM), and SEM-cathodoluminescence for gaining more information about the surface morphology. After this characterization, a thick GaN layer was grown on GaN substrates using molecular beam epitaxy (MBE). In order to understand the nature of these defects on the GaN substrates, the morphology was investigated before and after GaN growth. Following growth, the as-grown films were studied by both AFM and transmission electron microscopy (TEM) in order to know how these defects affect the growth, and if any negative effects can be mediated.

1.2 Background

1.2.1 Material Properties

Gallium Nitride has desirable physical, chemical, and mechanical properties. One of the properties of GaN is that GaN can withstand high temperatures with a large thermal conductivity. GaN has a direct wide band gap at 3.4 eV, which is considered high compared with other semiconductor materials (Table 1) [10]. The molecular weight of GaN is 83.74 g/mol, and the density is 6.15 g/cm^3. The compound is non-flammable and has tetrahedral coordination geometry. The mechanical properties are: melting point of 2500 °C, specific heat of 0.49 J g^{-1} K^{-1}, and bulk modulus of 20.4 x 1011 dyn cm^{-2} [9]. Electrical properties are as follows: electron mobility of ≤ 1000 cm^2 V^{-1} s^{-1}, electron diffusion coefficient of ≤ 25 cm^2 s^{-1} and intrinsic carrier concentration of 1x10^{10} cm^{-3} [7], [11] .

Table 1. Comparison between semiconductor material band gaps.

Material	Bandgap (eV)
Si	**1.11**
Ge	**0.66**
GaAs	**1.43**
GaSb	**0.70**
InP	**1.35**
GaN	**3.44**
CdS	**2.48**

1.2.2 Structural Properties

There are two structures for which GaN crystalizes naturally: cubic zinc blend face centered cubic (FCC) and wurtzite hexagonal close packed (HCP). The structure of cubic zinc blend consists of two FCC lattices that are interpenetrated [12]. These two FCC lattices consist

of Ga and N atoms which are interpenetrated and separated by a vector τ where τ = a (1/4,1/4,1/4). Here, a is the lattice constant between the atoms (Figure 2a). The wurtzite structure contains of two lattices of HCP that are interpenetrated with Ga atoms in one HCP and N in the other HCP. The lattices of HCP are separated by a vector τ = (0,0,5c/8), where c here is the lattice constant which is vertical (Figure 2b). There are four atoms per unit cell in the wurtzite structure, which is a hexagonal Bravais lattice [13]. As shown in Figure 2b, a is the length of the hexagonal base, c is the height, and u is the fraction of the c lattice length which separates the Ga and the N atoms along c-axis. The wurtzite HCP structure is found to be more electrically stable than the cubic zinc blend FCC. Therefore, wurtzite HCP is better for devices compared to cubic zinc blend FCC [14],[15],[7].

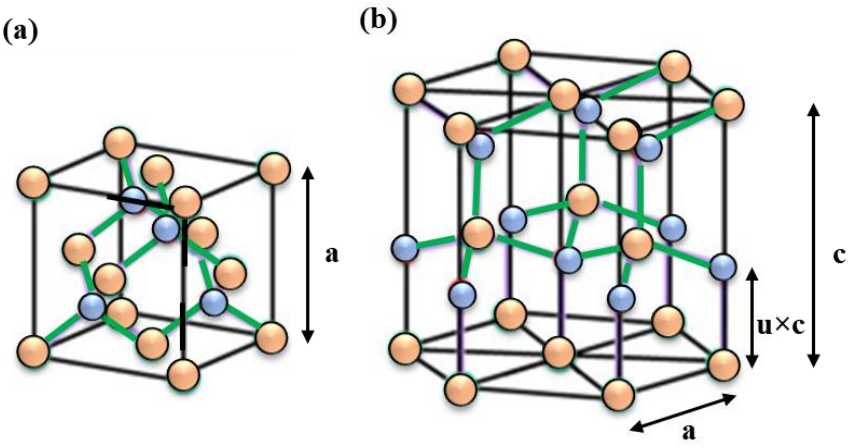

Figure 2. a) GaN structure of cubic zinc b) GaN structure of wurtzite.

1.2.3 Electrical Properties

Gallium nitride is a semiconductor material that has unique physical and electrical proprieties, which can be beneficial for high output power applications. GaN's wide bandgap energy supports high internal electric fields of 3.3 MV/cm [16]. Thus, it prevents breakdown and

results in enhanced radiation resistance. In addition, GaN has a low dielectric constant. The device terminal impedances can be impacted and lead to the capacitive loading capability of a transistor by the dielectric constant. GaN has high thermal conductivity allowing for power to be dissipated from devices thus avoiding high temperatures and thermal break down [17], [18].

1.3 Defects and Threading Dislocation in GaN

1.3.1 Dislocations

Dislocations are defined as changes of the ideal atom order in a solid. Dislocations can occur when the atoms are misaligned or when there is an atom missing, which is called a vacancy. The dislocation core can be caused by distorting the interatomic bonds in the immediate vicinity of the dislocation line [20] [21]. Minor variable deformations of the lattice at long distances are one of the dislocations which can cause lattice distortion positioned around a line. The Burger vector (b) is used to characterize the dislocations. The Burger vector b is the description of the slip distance in terms of the direction and magnitude [22], [23]. The dislocations are divided to three general categories: edge dislocations, screw dislocations, and mixed (edge-screw) dislocations. The edge dislocation is a line defect which is accompanied by lattice distortion and, hence, a lattice strain around it (Figure 3a) [24]. The Burger vector is perpendicular to the line defects in the edge dislocation [22]. The screw dislocation is essentially a shearing of one part of the crystal in relation to another part by atomic distance (Figure 3b) [24]. The Burger vector is parallel to the line defects in the screw dislocation. The mixed dislocation is a generalization, which includes components of both edge and screw dislocations (Figure 3c) [25].

1.3.2 Lattice Constant Mismatch

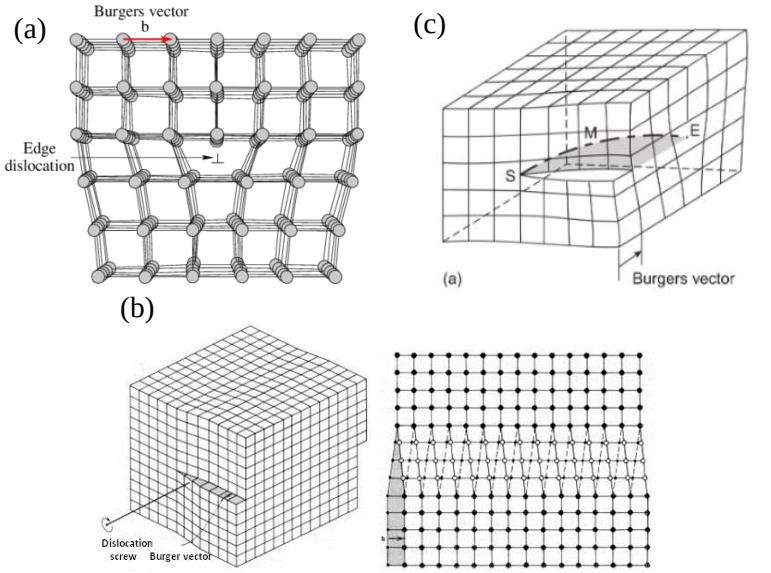

Figure 3. a) Diagram showing an edge dislocation, b) a diagram showing a screw dislocation, and c) a diagram showing mixed dislocations, which contain both edge and screw components.

Mismatched lattice constants result from epitaxial growth of a film on a substrate with a different lattice constant. Ultimately, this can cause defects in the crystal. This mismatched lattice constant results in strain in the crystal. It can be tensile strain when the film expands to match the lattice of the substrate, or compressive strain when the film contracts on the substrate [20], [6]. In other words, tensile strain results from the lattice constant of the film being smaller than the lattice constant of the substrate (Figure 4a) [26], and compressive strain results from the lattice constant of the film being larger than the substrate lattice constant as shown in Figure 4b [27].

1.3.3 Surface Morphology

The surface morphology of GaN substrates can be affected by several things, such as the dislocations in the structure or the growth conditions. Since GaN is grown on foreign substrates such as sapphire and silicon, the mismatch between GaN and the growth substrates can impact

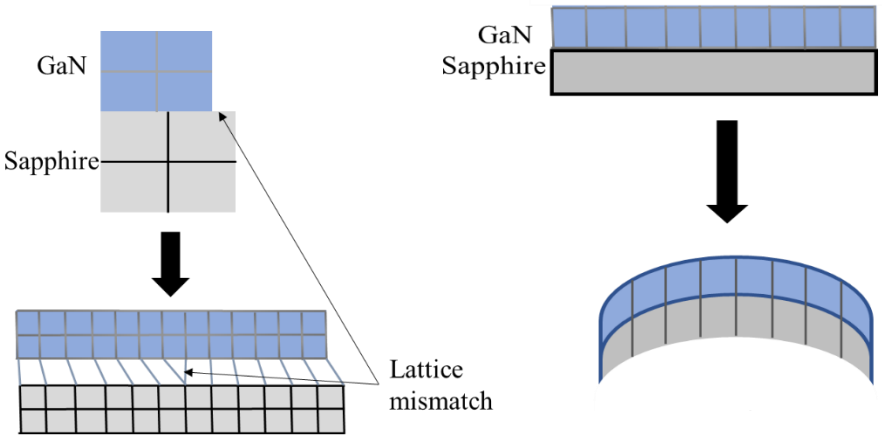

Figure 4. GaN substrate on sapphire showing a) the tensile strain and b) compressive strain.

the surface morphology of GaN which can affect the subsequent growth and the device performance. Dislocations in the structure can cause numerous defects on the surface such as hexagonal inverse pyramidal pits, hillocks, bumps and hexagonal facets [21].

As the crystal is grown, the dislocation inside the pit spreads in the direction of the center of the pit. The dislocation is centered in the hexagonal inverse pyramidal pits (Figure 5) [5], [21]. The hexagonal inverse pyramidal pits are clear from the dislocation except at its center [28]. These hexagonal pits can have different size, typically from a few nm to 100 μm.

Additionally, the dislocation can appear as a hexagonal hillock (Figure 6a) [29]. These hexagonal hillocks can contain many pits in its apex (Figure 6b) [30]. The pits can be considered as the end of a dislocation. Therefore, the dislocation can be surrounded by the hexagonal hillocks. The number of pits indicate the number of line dislocations in one hexagonal hillock [30] [31].

1.4 Hydride Vapor Phase Epitaxy

Hydride vapor phase epitaxy (HVPE) is a growth technique that is employed to produce

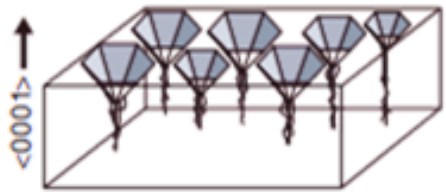

Figure 5. Dislocations centered in the hexagonal inverse pyramidal pits.

(a) (b)

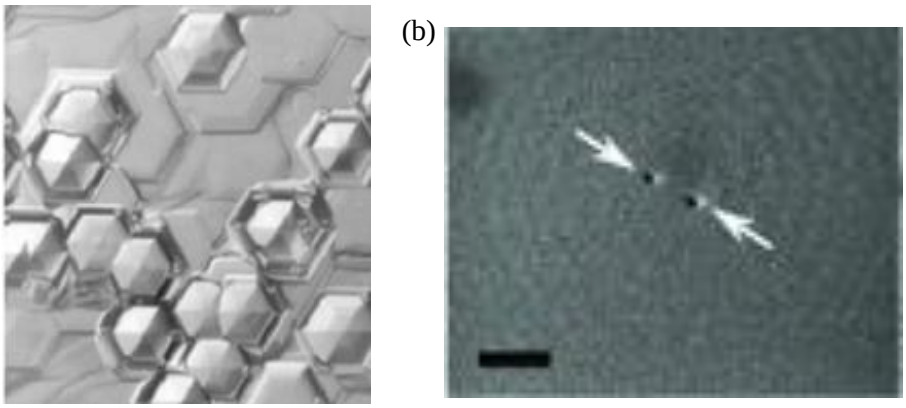

Figure 6. a) Shape of hexagonal hillocks in GaN surface and b) apex of hillocks which indicate the end of dislocations.

high quality thick crystals. This technique is used to produce semiconductor materials such as GaN and GaAs. HVPE is considered a promising technique to produce GaN on a foreign substrate such as sapphire. One of the most significant advantages of the HVPE technique is its high growth rate, which can be as high as ~100 μm/hour. In comparison to other epitaxial growth techniques, HVPE works under conditions of low pressure and growth temperature, while being relatively inexpensive [5],[32].

The common process of HVPE GaN growth involves two reactions. The first reaction is at comparatively low growth temperature, when the formation of chloride gas for the group three (III) metal is formed. The second reaction forms the nitride film at a higher temperature, when the chloride metal reacts with ammonia. For this, dual temperature zone reactors are used.

However, additional reactions can be used when creating doped materials. N-type GaN, p-type GaN, and semi-insulating GaN can also be grown by the HVPE technique. For n-type, silicon (Si) is added. For p-type growth, either magnesium (Mg) or zinc (Zn) is used. And, for semi-insulating GaN, to achieve a low carrier concentration, the background n-type material is doped with iron (Fe). In each case, the dopant is added in the low temperature zone to form a similar chloride before reacting with the surface of the GaN crystal [33], [3].

Chapter 2: Experimental Methods

2.1 Atomic Force Microscopy

Atomic Force Microscopy (AFM) is one characterization technique of Scanning Probe Microscopy (SPM) with possible resolution on the order of less than a nanometer. AFM is used to characterize the surface properties of materials from the atomic level to the micron level. A flexible cantilever with a pointed tip (probe) is the critical part of the AFM that is used to scan the sample surface line by line. The device measures the deflection of the cantilever while it scans, and the image is built up during the tip scanning. The central focus of the AFM working principle is that the cantilever deflection is affected by the force between the tip and the surface, which can be either attractive or repulsive.

To produce an image, the cantilever deflection needs to be detected and then converted to an electrical signal. A laser beam is used in the detection system. From the back of the cantilever, the laser is reflected to a position sensitive detector (Figure 7). The cantilever and the probe are made of either silicon or silicon nitride, and the tip radius of curvature, which governs its resolution, is generally a few nanometers to tens of nanometers. AFM depends on the force between the tip and the sample. Therefore, forces affect the image of AFM. These forces can be modeled using Hooke's Law (Equation 1) which indicates that when the tip is close to the surface of the sample, the cantilever is deflected.

$$F = -kz \qquad \text{(Equation 1)}$$

Where F is the force between the tip and the sample, k is the stiffness of the cantilever, and z is the distance between the tip and the sample. There are three modes of operation in AFM to characterize the sample: contact mode, non-contact mode, and tapping mode. In each mode

the cantilever oscillates at a different frequency [34]

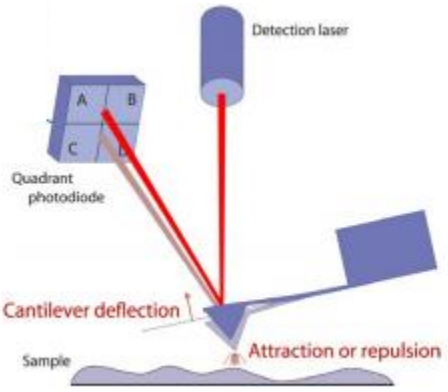

Figure 7. Schematic for atomic force microscopy.

In contact mode, a feedback loop is used to control the cantilever movement and correct the height of the cantilever depending on the height in the surface. The tip is pulled along the surface of the sample, and the surface is measured by using a cantilever deflection or using the feedback signal that requires the cantilever to be at a constant level (Figure 8a). The second mode is tapping mode, which is the most common mode that is used to characterize the surface. In tapping mode, the height and the setpoint amplitude are adjusted throughout the feedback system [34], [35]. In this mode, the tip creates repulsive connections with the surface of the sample, while the cantilever fluctuates (Figure 8b). The third mode is non-contact mode. In this mode, there is no connection between the tip and the sample (Figure 8c) [34].

In this research, AFM was a supportive technique to characterize the defects on the surfaces of four different substrates with particular parameters. The tapping mode was used to study the surface morphology. The height of these characterizations ranged from 10 to 200 nm. Z-limit was from 2 to 5 μm, and the scan size ranged from 2 to 70 μm. To get high quality images, the sample/line was 512, and the scan rate was low from 0.3 Hz to 0.5 Hz as summarized in Table 2.

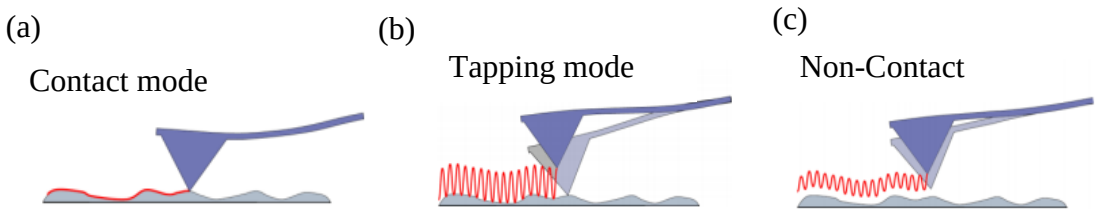

Figure 8. (a) AFM contact mode, (b) tapping mode, and (c) non-contact mode.

Table 2. Summary of the parameters that used in this research.

Mode	Height	Z-Limit	Scan Size	Sample/Line	Scan Rate
Tapping	10-200 nm	2-7 µm	2-70 µm	512	0.3-0.5 Hz

2.2 Scanning Electron Microscopy

Scanning Electron Microscopy (SEM) is a type of microscopy that uses electrons to characterize and analyze the microstructure morphology of a sample. The fundamental principles of SEM are similar to the optical microscope principles. However, the light source in optical microscopes is replaced by an electron beam with high energy. To form an image in SEM, the electron beam and sample interactions produce signals. These signals contribute in forming the image. There are two different interactions, which are elastic and inelastic interactions. The sample atomic nucleus can cause the deflection of the incident electron which can cause elastic scattering. This type of reaction is characterized by a small loss of energy through the collision, and it has a wide-angle shift of the scattered electron.

When the electrons are elastically scattered with an angle greater than 90˚, they produce a good signal to form an image of a sample. However, a large fraction of the incident electrons are scattered inelastically, losing as much as all of their kinetic energy. [36]. Consequently, these

secondary electrons (SE), which have a low energy that is less than 50 eV comprise a large portion of the reflected electrons and help in producing and characterizing an image of a sample [37], [38].

SEM was considered a helpful technique in this research. The main idea of using SEM was to study and analyze the substrates. Then, compare the results with AFM results. Also, SEM was used to see some defects that were not shown by AFM by using high magnification ranging from 90000x to 300000x. Figure 9 shows the SEM that was used in this research.

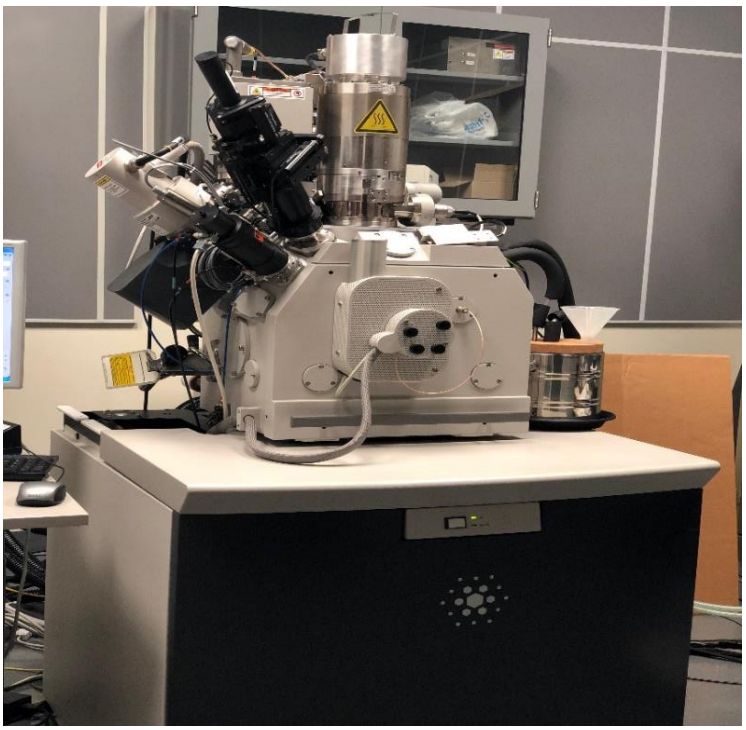

Figure 9. Scanning electron microscope.

2.3 Optical Microscopy

The most common type of microscope is an optical microscope that uses visible light and magnifies images by using lenses. Optical microscopy can even capture small objects and magnify them. In the optical microscope, the main parts are an objective lens and eyepieces. The

function of an objective lens is to magnify an object or defect. Therefore, the user can visibly observe the object or defect. The process to image an object by microscope is by locating the sample on the object space which is close to the objective lens focal plane. When the sample is located close to the focal plane, the magnified image of an object will be created on the middle plane which is positioned on the focal plane of the eyepieces. Then, the function of the eyepiece is to magnify the image further, so the user can see it clearly [39], [40], [41]. The Olympus BX60 (Olympus Corporation, Tokyo, Japan) was used in this research. The main reason to use an optical microscope was to study the morphology of GaN substrates and to calculate the defect density on GaN surfaces. Also, optical microscope results and images were compared with other microscopes such as AFM and SEM. There were three magnifications lenses used in this research 5x, 10x, and 20x.

2.4 X-Ray Diffraction

X-ray diffraction (XRD) is a characterization technique which uses electromagnetic radiation in the x-ray regime, here with a wavelength of 0.15406 nm, to probe the crystal structure. XRD generally utilizes radiation (λ) with a wavelength near the crystalline lattice spacing. X-rays are generated by a metal extrusion with electrons in a vacuum tube, and the x-ray is frequently chosen to be monochromatic [22]. Electrons that are around atoms scatter x-rays in several directions with the same frequency which contribute to create constructive interference as shown in Figure 10. Bragg's law indicates that the distance between planes of atoms is related to the incident beam angle (Equation 2) [22], [42].

$$n\lambda = 2d \sin\theta \qquad \text{(Equation 2)}$$

where λ is the x-ray wavelength, d is the distance between planes of atoms, and θ is the incident

and reflected beam angle. There are several scan types that are used in XRD characterizations. ω-scan is used to measure the quality of the material and can determine the dislocation density and sample curvature. ω-2θ and 2θ-ω scans are used to detect the lattice parameters of the material.

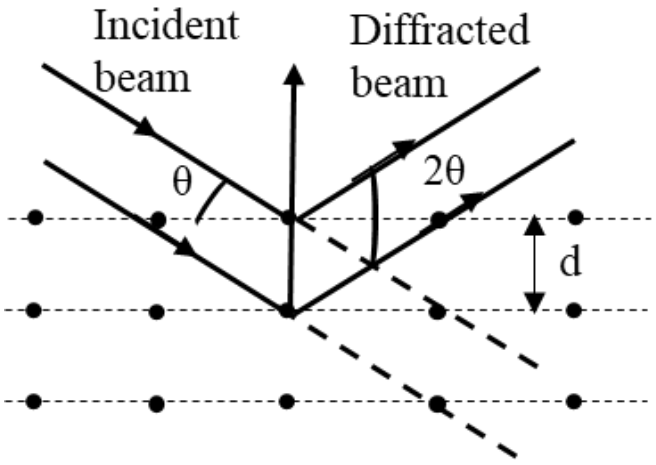

Figure 10. Constructive interference between planes occurs at a certain angle.

In this research, XRD characterization was important to understand the defects in the structure and detect the dislocation density in the GaN substrates. ω-scans were used to investigate the structural quality of the GaN. ω-scan was applied in (002) and (102) directions to study different types of dislocations [22], [43].

The XRD peak width is related to the crystallite size, and it can be the result of many mechanisms. An infinitely large, perfect crystal has, ideally, a peak width limited only by the instrument [44]. Generally, broadening of the peak can be characterized by the following values: the broadening of the instrument β_d, strain and dislocation in the structure β_ε, wafer curvature β_r, the rotation of the lattice to dislocation by either tilt or twist β_α, the limited correlation length β_L, and the crystal essential rocking curve β_o as given in Equation 3 [22].

$$\beta_{FWHM}^2 = \beta_o^2 + \beta_d^2 + \beta_\alpha^2 + \beta_\varepsilon^2 + \beta_L^2 + \beta_r^2 \quad \text{(Equation 3)}$$

The crystal essential rocking curve and the broadening of the instrument are small compared with other broadening. The broadening of the instrument is the diffractometer characteristic that is employed for the experiment [44]. However, since it is small, it will not have much effect on the broadening. In contrast, defects and strain in the structure that can be caused by vacancies, mismatch of lattice constant, and threading dislocation density are essential causes of increasing the broadening. The tilt and twist to the dislocation can affect the broadening. These dislocations can be screw dislocations, edge dislocations, or mixed dislocations that contain both screw and edge dislocations. Moreover, the wafer curvature that can be affected by the strain and unrelaxed film can increase the line width of the broadening. This wafer curvature is a result of the different lattice constant between the GaN and sapphire interface. Another influence of the broadening is the correlation length, which is defined as the measurement of the crystal long range order. This indicates the length at which the crystal unit cell is duplicated as expected. The crystallite size is usually indicated by the correlation length. However, the disarranged bulk crystal can consist of numerous individual crystallites [22],[44].

2.5 Transmission Electron Microscopy

Transmission electron microscopy is one of most useful imaging techniques to study, characterize, and analyze materials by using high magnification and resolution. The working principle of the TEM is different than the optical microscope. In order to produce an image by TEM, a focused beam of high energy electrons is used instead of light. The resolution of images in TEM is significantly higher than those of optical microscopes. Therefore, microstructural details in the range of a few tenths of nanometers can be examined by high resolution imaging.

Moreover, TEM is used to investigate the structure and orientations of the crystal [45], [46].

The FEI Titan 80-300 TEM (FEI Company, Hillsboro, OR) at the University of Arkansas was used in this research is shown in Figure 11. It was used to study a thick growth of GaN on GaN/sapphire substrates and to investigate if the defects on the substrates have any impact on the subsequent growth.

Figure 11. FEI Titan 80-300 TEM.

2.6 SEM-Cathodoluminescence (SEM-CL)

SEM-cathodoluminescence (SEM-CL) is a method in which photons with particular wavelengths are produced from material emitted by high-energy electrons and produced by an electron gun in a scanning electron microscope. This technique works in different ways depending on the structure or if there is any defect or damage subsequent in a variation of structure. This technique can be understood from the band theory in the solid state which indicates that an insulator such as quartz has a conduction band and a valence band. These bands are separated by a band gap. If an electron with enough energy hits a crystalline structure to

excite an electron with high energy from the lower valence band to the conduction band, the excited electron returns immediately to the valence band in non-excited state.

This electron can be reserved for a short time in the either intrinsic or extrinsic impurities such as the defects and traps. Energy will be produced when the electron is released from these defects or traps. This energy can result in luminescence when it is in the range of the required wavelength. In this way, the electrons are trapped and released with different energy resulting luminescence [47], [48].

SEM-CL characterizations were applied on GaN substrates to know how these spectra would be affected by the defects in the surface and structure. Much individual and mapping CL characterization was done with 10 sec for each pixel. Each pixel had a complete spectrum.

2.7 Photoluminescence Measurement

Photoluminescence (PL) measurement is an appropriate technique to characterize the optical properties of semiconductors materials. The working principle of PL is that a laser with energy higher than the band gap excites carriers from the valence band to the conduction band. The recombination between the electron and hole will be done when the carriers relax into a state that has lower energy which subsequently results in the emission of a photon. The recombination between the electron and hole results in radiative light which can be detected by the PL measurement. PL measurement can be done at room temperature and low temperature. At room temperature, the recombination that is not radiative can be active. The low temperature measurements were used to decrease the impact of the lattice vibrations. In PL, a laser source is used such as a HeCd Laser, and its wavelength is 325nm. This laser is used to excite a photon with energy higher than the band gap of the materials [49]. Figure 12 shows the setup diagram of

PL used in this research.

In this research, PL measurement was a critical technique for optical characterization of GaN substrates. Also, PL measurements helped to determine if the band gap of GaN had been affected

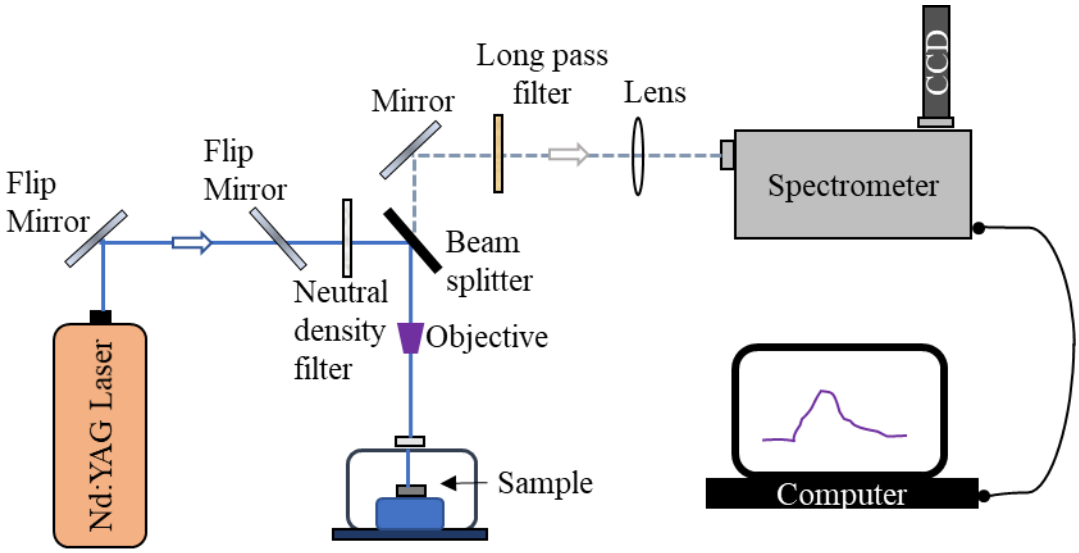

Figure 12. Setup diagram of low temperature PL.

by the defects or not. The wavelength in those measurements ranged from 300 to 500 nm since the GaN absorption wavelength is approximately 340 nm. The measurements were done at low temperature, which ranged from 16 K to 18 K. The time was 20 sec, and the slit sizes that were used were 0.1 mm, 0.2 mm, 0.05 mm.

2.8 Optical Transmission

Optical transmission measurement of a semiconductor provides valuable insight to the quality of optical material by transmitting radiation to the material versus wavelength. The light source radiation either transmits through a material interface or reflects from it. The radiation energy entering the sample will be absorbed if it is equivalent to or greater than the

semiconductor band gap. The non-absorbed radiation travels to the semiconductor interface where it either exits from the semiconductor or is reflected again. Reflected radiation can be reflected inside again at the first interface and then again at the exit interface resulting in numerous reflections, each one crossing a different path length, and thus each one varying in phase [50].

The measured transmission exiting results from those numerous reflections when they are constructive or destructive with each other. The measured transmission quickly reduces to zero when it is near the band gap, and the absorption increases sharply. This indicates that the material has a high quality structure. For a transmission measurement instrument, a detector and standard light source are essential to measure transmittance of the materials. The transmission measurement process normally involves two steps. The first step is to measure the standard light source with the air and without the material. The second step is to measure with the material. The ratio of these two measurements is the transmission of the sample (Equation 4) [50].

$$T = \frac{Isample}{I\ refernce\ (air)} \qquad \text{(Equation 4)}$$

Transmission measurement was a valuable measurement to get more optical information about GaN on sapphire substrates. The band structure was studied by the transmission measurement. Also, transmission measurement was used to investigate whether defects and dislocation densities had any effect on GaN, especially its optical properties.

Chapter 3: Results and Discussion

3.1 Unintentionally Doped GaN on Sapphire with Titanium

An HVPE unintentionally doped GaN on sapphire (UID1) substrate was coated with 1 μm of titanium (Ti) using electron beam evaporation (Figure 13). UID1 is a 2-inch diameter sapphire wafer with 5 μm of HVPE grown GaN on one side which has been polished in order to promote good epitaxy. The other side is mechanically rough. It is on this side that the Ti coating was performed. The aim of coating Ti on the backside of UID1 substrate was that after characterization of UID1 substrate, a thick layer of GaN needed to be grown by molecular beam epitaxy (MBE). In the MBE chamber, a filament which is made from tantalum or conductive graphite is used to heat the substrate. However, GaN-on-sapphire, which is visible and infrared transparent, does not absorb enough thermal radiation from the substrate heater filament in the MBE. Therefore, a high temperature metal, typically Ti, is used as a backside coating to increase the heat radiation absorption during the growth [51]. After coating Ti on the backside of UID1 substrate, several types of characterization were performed on the substrate.

Figure 13. GaN with no coating (left) and GaN with backside coated with Ti (right).

3.1.1 Morphology Characterization

Atomic Force Microscopy

Atomic Force Microscopy (AFM) measurements were done on the UID1 substrate. AFM is essential to characterize the surface quality, roughness, and the densities of various defects on the substrate. The characterization was done by using a silicon tip with a small radius of curvature of approximately 10 nm. The surface of UID1 was investigated in many different places to investigate the uniformity of the surface. There were three types of defects: small pits, big pits, and ridges. Figure 14 shows a smooth AFM image for UID1 with small pits (less than 1 μm width and 3 nm depth). The roughness in this area was 1.02 nm. Comparing with another area, Figure 15 shows that the surface had some small pits and big pits. Those small pits were around 10 nm in depth, and the width of them was approximately 0.15 μm. For the big pits, the depth was around 30 nm, and the width was around 1.5 μm. The large pit density was about 7.5 $\times 10^3$ cm^{-2}. Those pits affected the roughness of the surface by increasing the value of the roughness to 4.35 nm in that area.

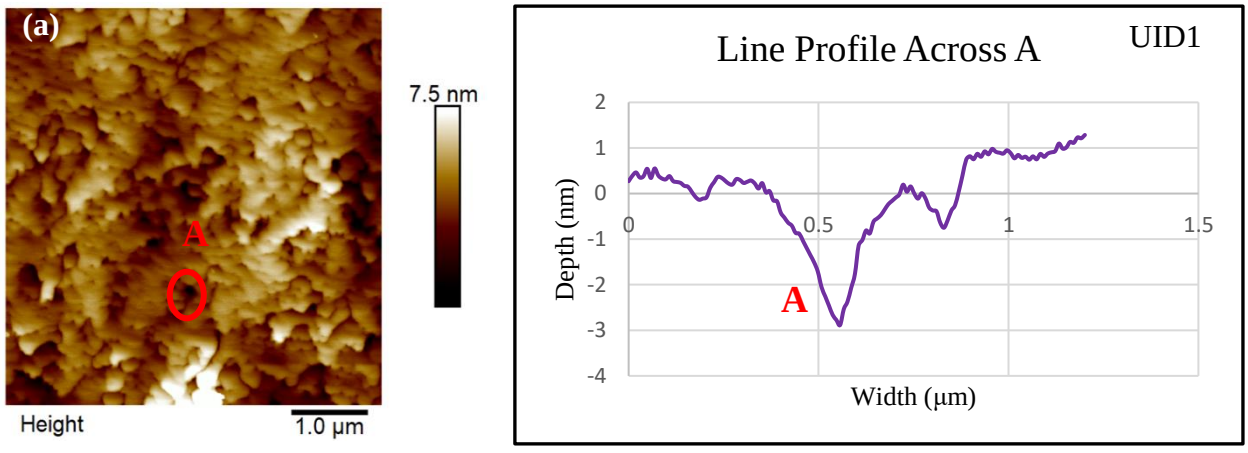

Figure 14. AFM image showing that UID1 suffered from a high density of pits. The line profile is through the pit, which is circled in the left image.

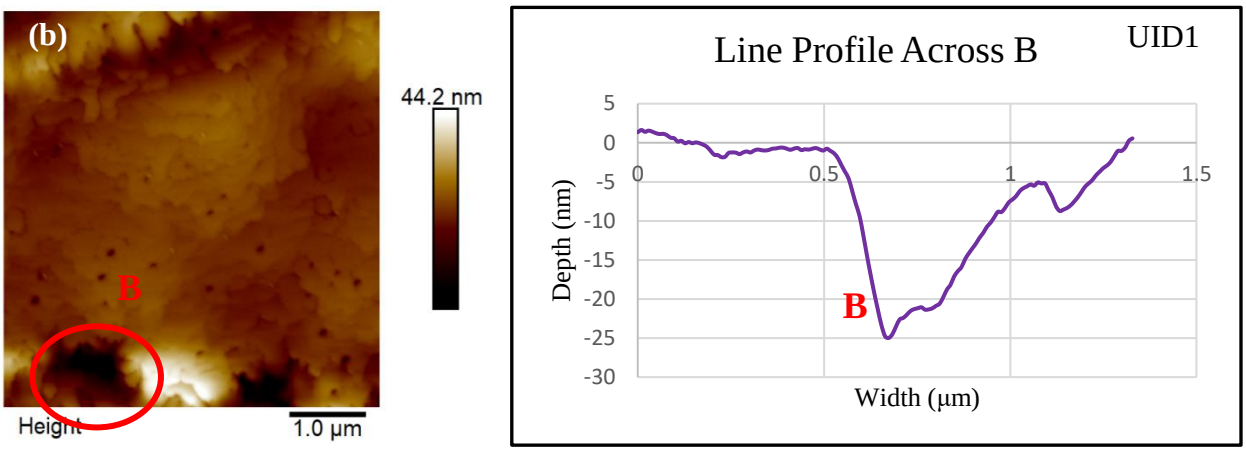

Figure 15. Large holes with width about 1 μm detected in UID1. The line profile is through the pit which is circled in the left image.

There are different types and sizes of pits which appeared to spread randomly on the surface. In order to characterize the density of those at different points on the surface, mapping the sample and counting the pits in different areas was done, resulting in an average pit density of approximately 8.55×10^{7} cm^{-2}. Equation 5 was used to calculate the pit density [52]. All scanning areas had the same size which was 5 × 5 μm.

$$D = \frac{n}{a}, \qquad \text{(Equation 4)}$$

where D is the pit density, n is the number of pits in each image, and a is the area of the scanning surface. The cause of these different sizes of pits possibly is the threading dislocation in the structure of UID1 substrate. During the mapping, some very large-scale ridges were scanned (Figure 16). The surface consists of ridges with widths ranging from 2 to 4 μm. The roughness is 10.1 nm. In order to investigate these in a larger scale, a 40 μm image was scanned (Figure 17). The surface of the UID1 substrate was widely populated by these ridges which separated large terraces with widths ranging from 6 μm to 9 μm, and heights from 50 to 90 nm. The resulting

roughness became 37.3 nm. Table 3 summarizes the defects in UID1.

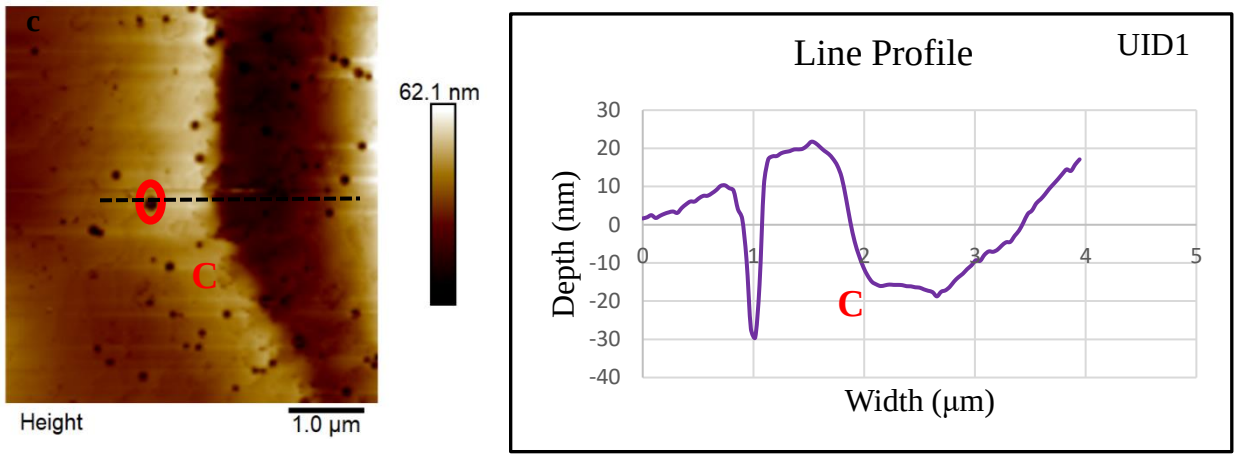

Figure 16. UID1 has pits distributed randomly and edges with step height about 20 nm. The line profile is through the pit and the edge that in shown in left the image.

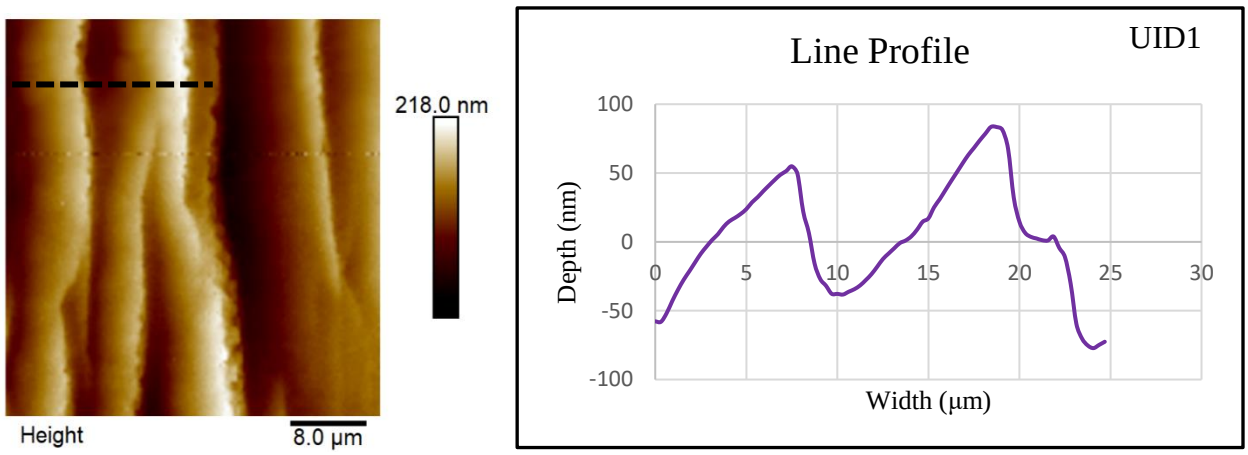

Figure 17. UID1 has large terraces with step height about 90 nm**.** The line profile is through the terraces as shown in the left image.

Table 3. Summary of roughness, pit density, average pit size, and average pit depth for UID1.

Image ID	Roughness (nm)	Pit Density (cm^{-2})	Average Pit size (µm)	Average Pit Depth (nm)
A	1.02	6×10^{7}	0.3	4.5
B	4.35	7.6×10^{7}	0.15	10
C	10.1	2.68×10^{8}	0.3	30

Scanning Electron Microscopy

In addition to AFM measurements, scanning electron microscope (SEM) images were obtained on the UID1 substrate. The measurement was done on the substrate to compare the AFM images with SEM images and calculate the defect density on the surface of UID1 substrate. Figure 18 shows the shape of the pits on the surface which were hexagonal V-shape pits. Unintentionally doped GaN substrates suffer from V-shape pits that can affect the subsequent growth [53]. These hexagonal V-shape pits were distributed randomly on the surface of the UID1 substrate with different sizes. The size of these hexagonal V-shape pits ranged from 30 nm to 200 nm in diameter (Figure 18).

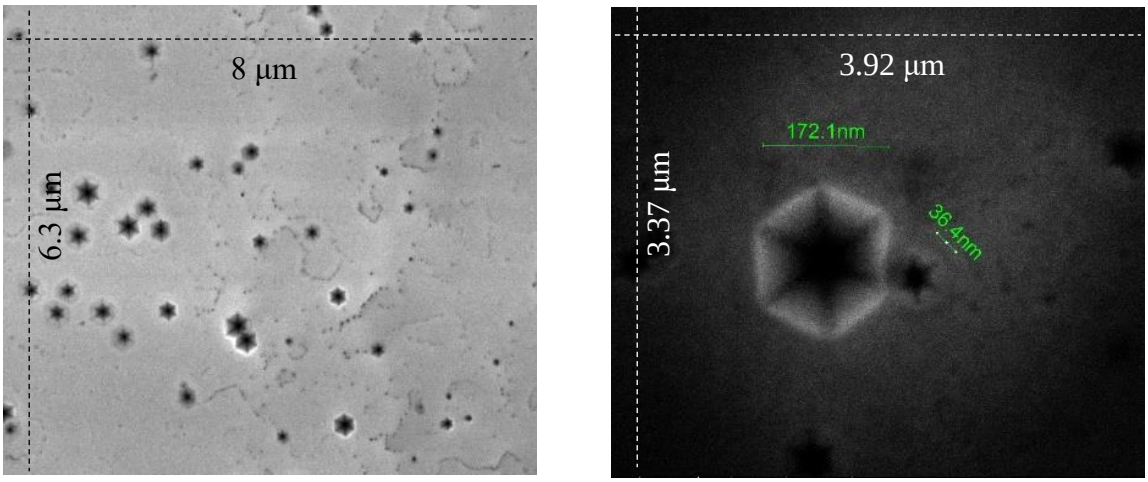

Figure 18. SEM image demonstrating the V-shape pits in UID1.

Some areas had these hexagonal V-shape pits and others appeared to be clear (Figure 19). To calculate the hexagonal V-shape pits, mapping the surface of UID1 was carried out. The size of the images was 13 × 16 µm. The defect density of the hexagonal V-shape pits was estimated to be approximately 1.65×10^{7} cm^{-2}, which was similar to the results estimated by AFM images. These V-shape pits are the termination of threading dislocations intersecting the surface

during growth.

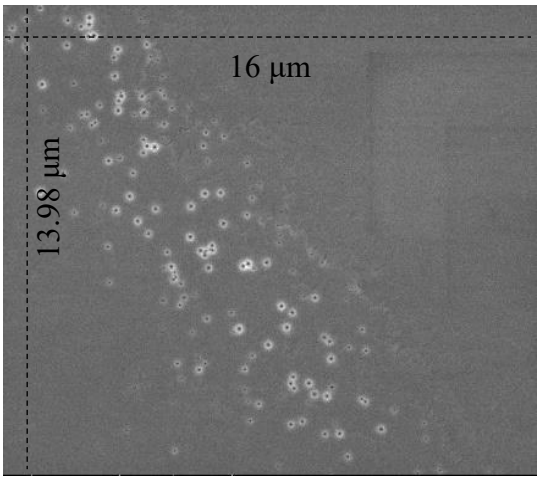

Figure 19. SEM image demonstrating the density of V-shape pits in UID1.

Optical Microscope

In addition to AFM and SEM measurements to investigate the surface morphology of the UID1 substrate, optical microscope images were obtained to analyze more defects in UID1 surface. Optical microscopy is an important technique to study a material surface over a large scale. By optical microscope, a new defect was observed. These defects were similar to the terraces on the surface. Their distributions were varied on the substrate as shown in Figure 20. UID1 substrate was mapped by optical microscope to estimate the terrace densities on the surface (Figure 20). The distribution of these defects was parallel to the flat side of the substrate. Figure 20b shows the terrace density on the left side of the sample for which the average was estimated to be 1.93×10^5 cm^{-2} in 683.19 μm × 499 μm size. The highest defect density was in the middle of the substrate which was approximately 3.22×10^5 cm^{-2} (Figure 20c). The lowest defect density was found on the right side which was calculated to be around 1.5×10^5 cm^{-2} (Figure 20d). The total defect density was approximately 2.20×10^5 cm^{-2}.

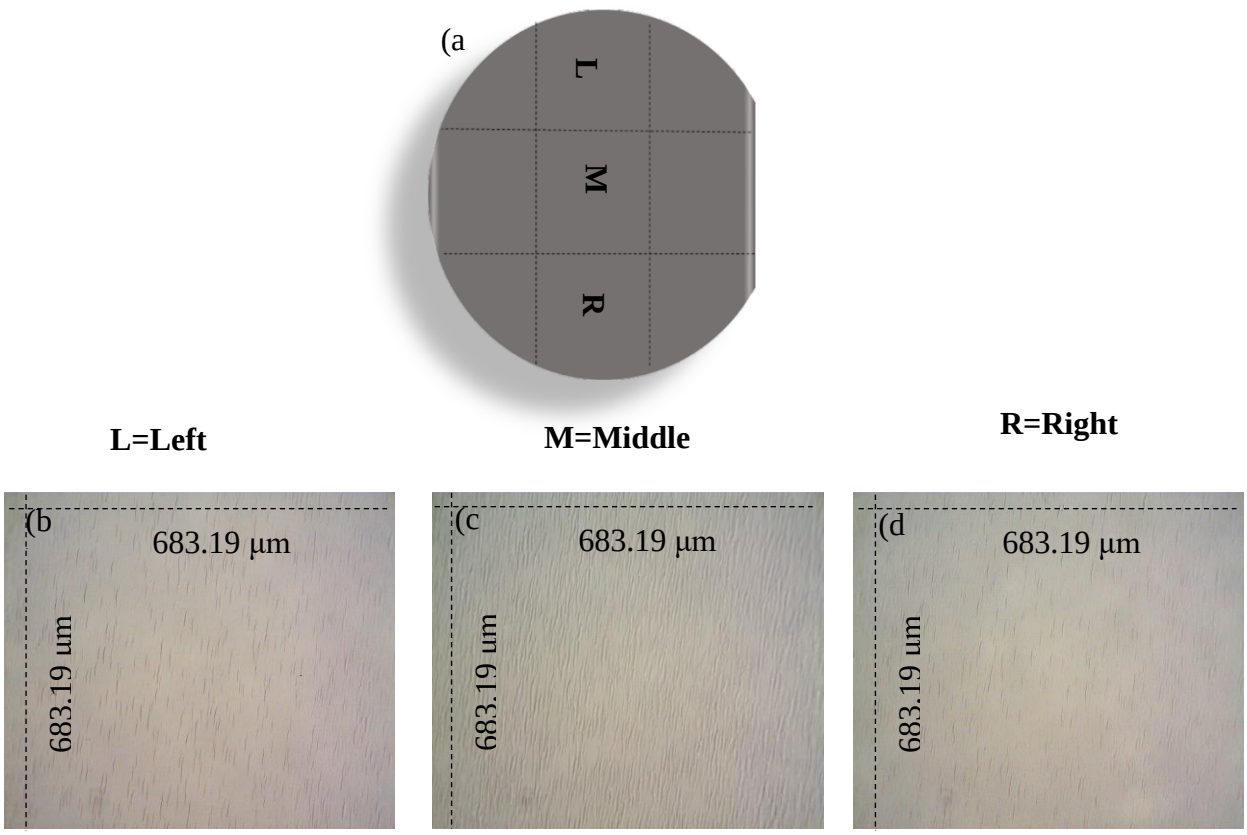

Figure 20. Optical microscope images of UID1 (a) showing the mapping of the substrate (b) illustrating the density of terraces in the left side, (c) demonstrating the terrace density in the middle, and (d) showing the lower terrace density in the right side.

In summary, the morphology of the UID1 substrate was studied by three different types of microscopy. AFM measurements were carried out to characterize the surface morphology. Three types of defects were observed by AFM which were small pits, big pits, and ridges on the surface. The total defect density of the small pits was 8.55×10^{7} cm^{-2}, and large pit density was 75×10^{2} cm^{-2}. The second microscopy was SEM. Mapping by SEM was performed to study the defects in UID1 substrate and compare them with AFM measurements. Hexagonal V-shape pits were detected by SEM. Those hexagonal V-shape pits had different sizes and were spread randomly in the surface. The total V-shape pit density was 1.65×10^{7} cm^{-2}, which was similar to the small pit density from AFM. The third microscopy was optical. Optical microscopy was used

to study the surface over a large scale (683.19 μm × 499 μm). New defects were observed that were not seen by AFM and SEM measurements. The density of those defects was high in the middle of the sample and lower in the edge of the sample. The average defect density of those terraces was 2.20×10^5 cm^{-2}.

3.1.2 Structural Characterization

X-Ray Diffraction

In order to investigate UID1 structure, many different characterization methods were performed. X-ray diffraction is a critical technique to investigate the UID1 substrate structure. There are several measurements that can be done by x-ray diffraction such as ω-scan, θ-2θ, and ω-2θ. The ω-scan (commonly known as a rocking curve) measurement is essential to measure the quality of the material and detect the dislocation density. The rocking curve ω-scan can measure the lattice tilt from screw dislocations for symmetric measurement, so it was performed to study (002) symmetric reflection (Figure 21). Also, the rocking curve ω-scan can measure twist from mixed dislocation, so it was performed to investigate (102) asymmetric reflections (Figure 22). In symmetric measurement for the screw dislocation, the Burger vector is parallel to the dislocation line. However, the Burger vector is perpendicular to the dislocation line in edge dislocation. Therefore, it is hard to measure the edge dislocation, so mixed dislocations were measured. From the peak width, the full width at half maximum (FWHM) could be calculated for (002) and (102) reflections which were 402 arcsec and 1709 arcsec for UID1, respectively. The FWHM is associated with lattice distortions, so the threading dislocation density could be calculated by using FWHM values. The square of FWHM is proportional to the dislocation density. The FWHM value for (002) and (102) reflections is associated with screw and mixed dislocations, respectively. To calculate the dislocation density from the FWHM, Equation 5 was

used.

$$D = \frac{\beta^2}{4.35b^2} \qquad \text{(Equation 5)}$$

$$b = \frac{a}{2}\sqrt{U^2 + V^2 + W^2},$$

Where D is the dislocation density, β is the FWHM, and b is the magnitude of the relevant Burger vector given by $\{UVW\}$, and a is the unit cell edge length. The screw dislocation density of (002) reflection was calculated to be 3.23× 10^8 cm^{-2}. The mixed dislocation density of (102) reflection was 1.53× 10^{10} cm^{-2}.

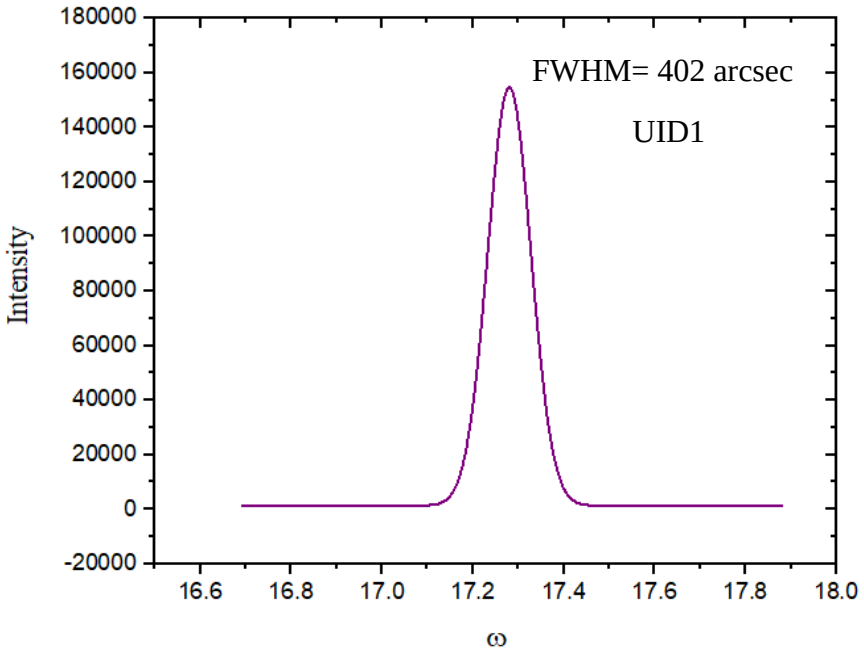

Figure 21. X-ray peak associated with screw dislocation from (002) plane reflections for UID1.

Cathodoluminescence

Cathodoluminescence (CL) is an important technique to study how the defects

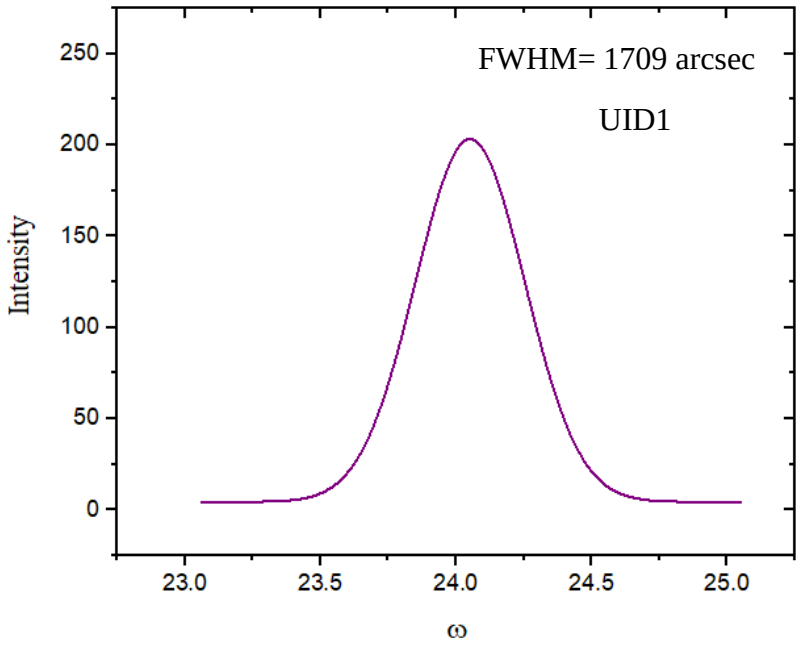

Figure 22. X-ray peak associated with mixed dislocation (102) reflection for UID1.

affect the optical properties in GaN substrates. Therefore, CL measurements were performed to investigate the dislocation in the substrate and their effects. Therefore, the measurements were taken in several areas to investigate the changing in the UID1 substrate optical properties and how these properties were affected by the structural and surface defects in the substrate. In this measurement, the electron beam energy was 10 KeV, the measurements were at low temperature, ~ 98 K, and the scanning areas ranged from 3 μm to 5 μm.

Figure 23 demonstrates two results of CL measurements. Figure 23a is a panchromatic CL image for the characterized area. This panchromatic imaging is the result of not spectrally resolving the light from the CL spectra that fell inside the exposure area. From Figure 23b, it is clear that the structure of UID1 was not uniform and contained defects and dislocations. Figure 23c is the SEM image of the investigated area. Figure 23a illustrates the CL spectrum for one of the dark spots. As shown, there was one peak. The peak was the near band edge

emission. NBE is at ~3.4 eV. The effect of the NBE energy can be associated with the high dislocation densities. Also, strain has effect on the near band edge energy. By studying several areas in the UID1, there was no other luminescence observed. However, the intensities did vary slightly. Figure 24 shows the CL spectrum in the light area. Figure 25 demonstrates the change in the intensities. The dark area had low intensities which indicated that the emission was weaker in those areas than the light areas.

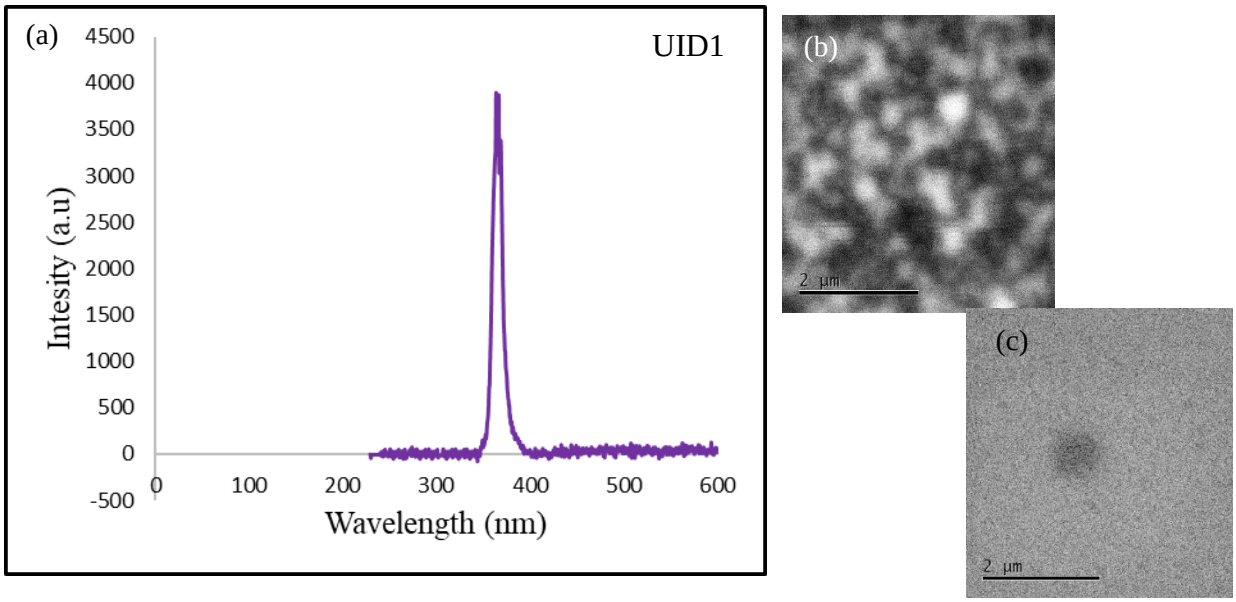

Figure 23. CL measurements of UID1 in the dark region: a) the CL spectra peak, b) panchromatic image, and c) SEM image.

3.1.3 GaN Growth on UID1

Many characterization procedures were performed on the UID1 substrate, and different defects were found on the surface of UID1 substrate and dislocations on the structure. Therefore, to know the effect of the defects and dislocations in UID1 substrate on the subsequent growth, UID1 was cut to four quarters, and 1 µm of GaN was grown on one quarter of UID1

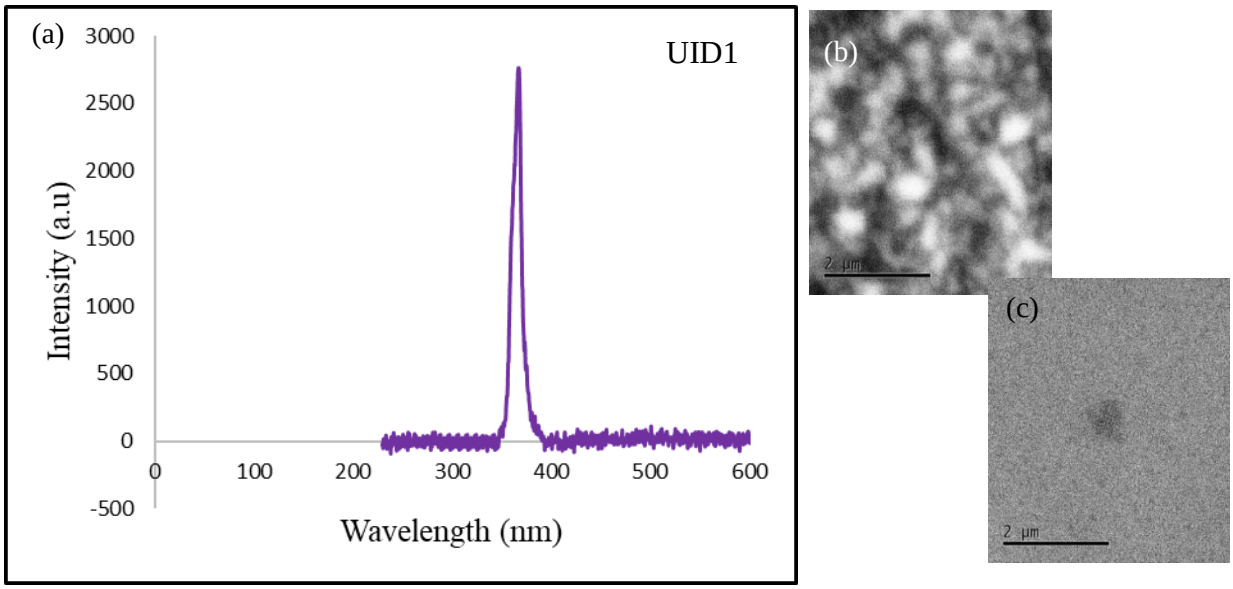

Figure 24. CL measurement for UID1 in the light region: a) the CL spectra peak, b) panchromatic image, and c) SEM image.

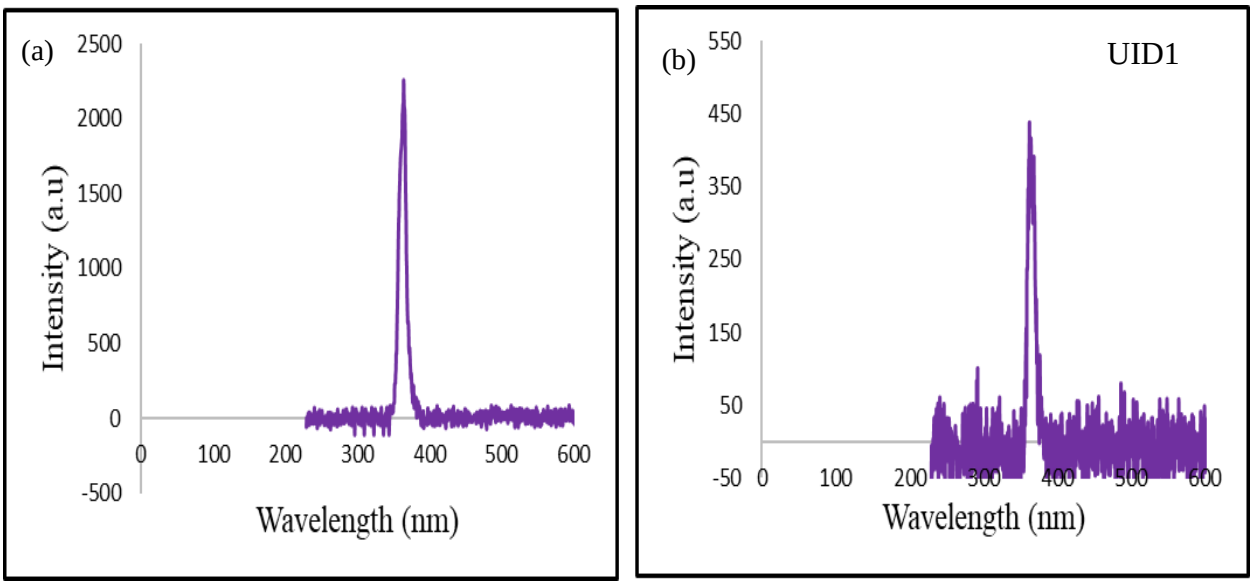

Figure 25. Comparison of CL measurements in the (a) light and (b) dark regions.

substrate by using molecular beam epitaxy (MBE) at 750 °C (Figure 26). Then, this subsequent growth was characterized by AFM and TEM.

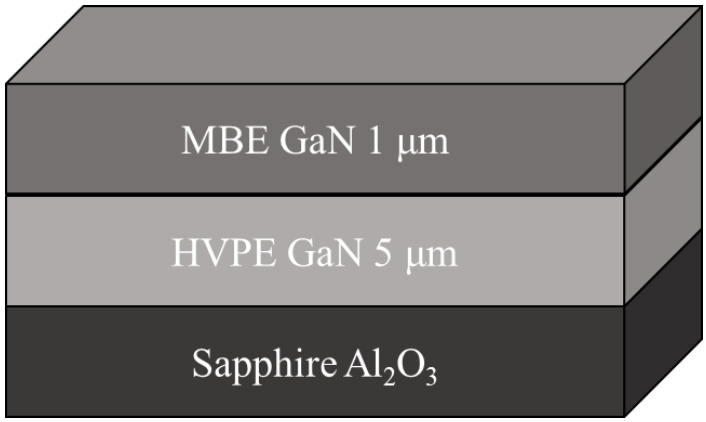

Figure 26. Scheme for the growth of 1 μm of GaN on UID1.

Atomic Force Microscopy

The surface of the as-grown GaN on UID1 substrate was then investigated by AFM similar to before the growth. Mapping the surface of GaN to investigate the whole sample and count the defect density was done for 5 × 5 μm size images. Many defects were detected on the GaN on UID1 substrate. As shown in Figure 27, the surface suffered from ridges with depth ranging from 10 to 40 nm and width ranging from 1 to 3 μm. These ridges were similar to the ridges before growth as shown in Figure 16. The roughness of this image was 10 nm. Moreover, similar to Figure 16, the same area contained some pits with pit density equal to 9.6×10^7 cm^{-2}. Even though the roughness was low at 1.58 nm in (Figure 28), this area not only had pits but also had some lines with length ranging from 0.2 to 1.7 μm with total length 25.43 μm. The pit density in this area was approximately 8×10^6 cm^{-2}. New defects were observed, distorted pits as shown in Figure 29 with pit density 2.84×10^8 cm^{-2}. These distorted pits had depths ranging from 15 nm to 20 nm and widths ranging from 0.1 μm to 0.3 μm. The roughness was 3.50 nm.

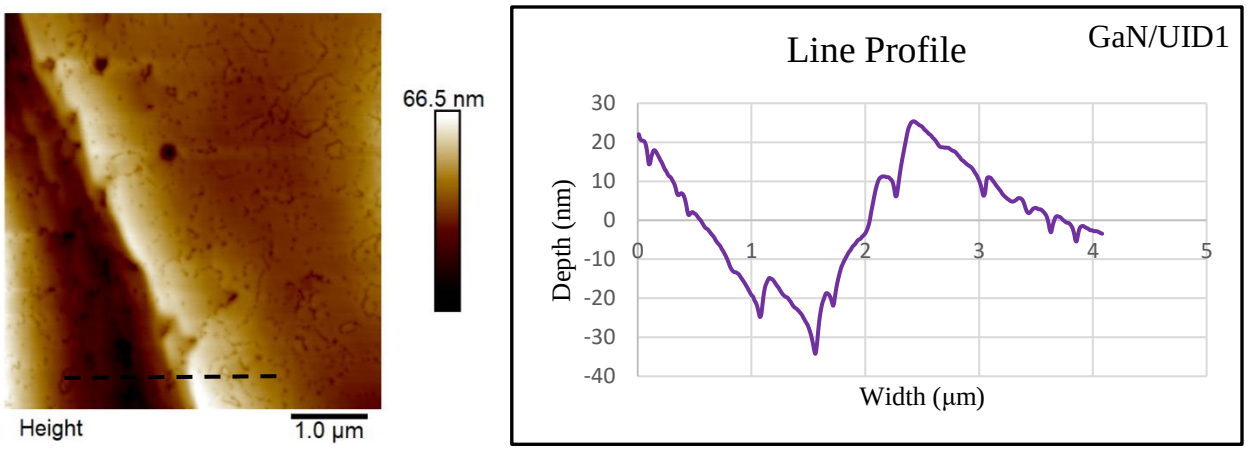

Figure 27. Large ridges with pits measured after GaN growth. The line profile is through the ridges as shown in the AFM image at the left.

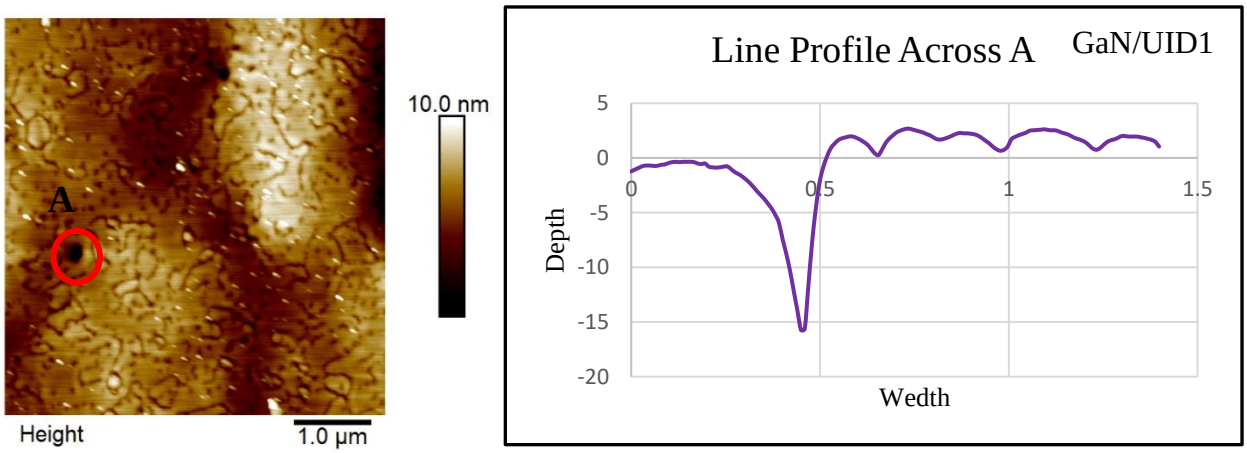

Figure 28. GaN layer with line defects. The line profile is across circle A in the AFM image at left.

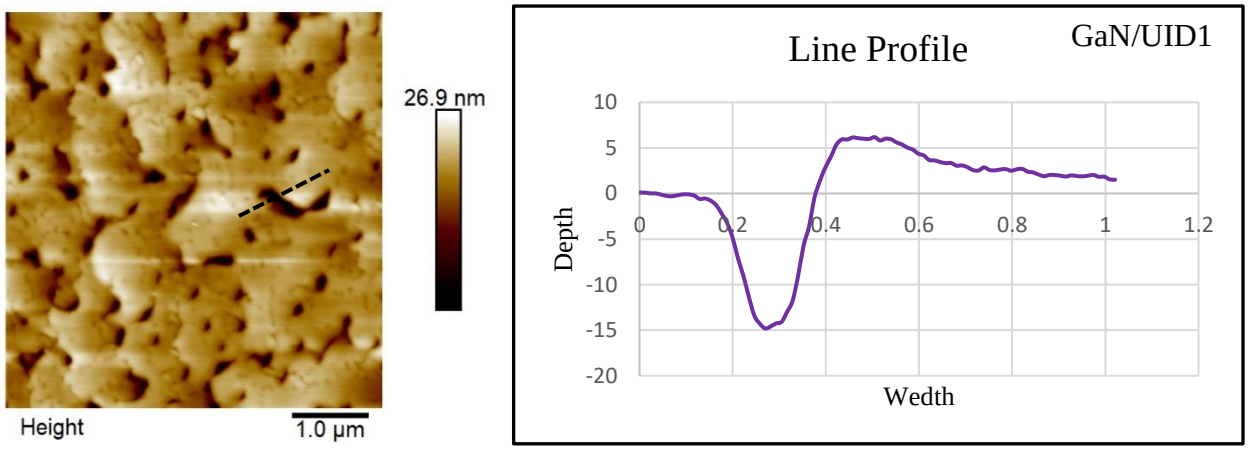

Figure 29. Distorted holes formed after GaN growth**.** The line profile is through the line drawn in the AFM image at left.

3.2 Unintentionally Doped GaN on Sapphire with no Titanium

The second HVPE sample, unintentionally doped GaN on sapphire (UID2) substrate with no Ti, was also investigated by several microscopy techniques for surface and optical characterization and for the structure quality. UID2 substrate was also a 2-inch sapphire wafer with a 5 μm thick layer of HVPE grown GaN on the polished surface. The surface morphology was characterized by AFM, SEM, and optical microscopy measurements. The quality of the structure was characterized by x-ray diffraction; optical characterization (transmission) was also performed on the UID2 substrate.

3.2.1 Morphology Characterization

Atomic Force Microscopy

AFM is essential to characterize the surface quality, roughness, and the various defect densities on the substrate. The characterization was done by using a silicon tip with a small curvature radius of approximately 10 nm. The surface of UID2 was investigated in many different places to determine the uniformity of the surface. Figure 30 shows a smooth AFM image for UID2 with small pits (less than 0.3 μm width and 2 nm depth). The roughness of this area was 0.939 nm. By taking a small scan size which was 2 × 2 μm, Figure 31 showed that the surface had some small pits. These small pits were around 1 nm to 2 nm in depth, and the width of them was approximately 0.15 μm. The roughness value of the surface in this area was low, approximately 0.379 nm. Mapping the surface was carried out to calculate the total pit density which was 8.9×10^{8} cm^{-2}.

Scanning Electron Microscope

In addition to AFM measurements, SEM measurements were performed on the

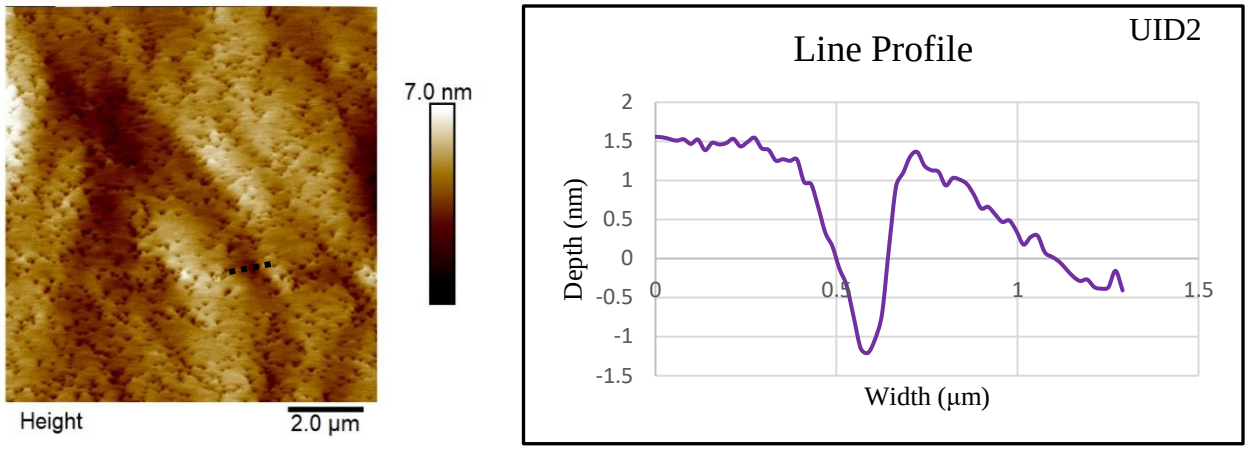

Figure 30. AFM image showing high density of pits. The line profile is through the drawn line in AFM image at the left.

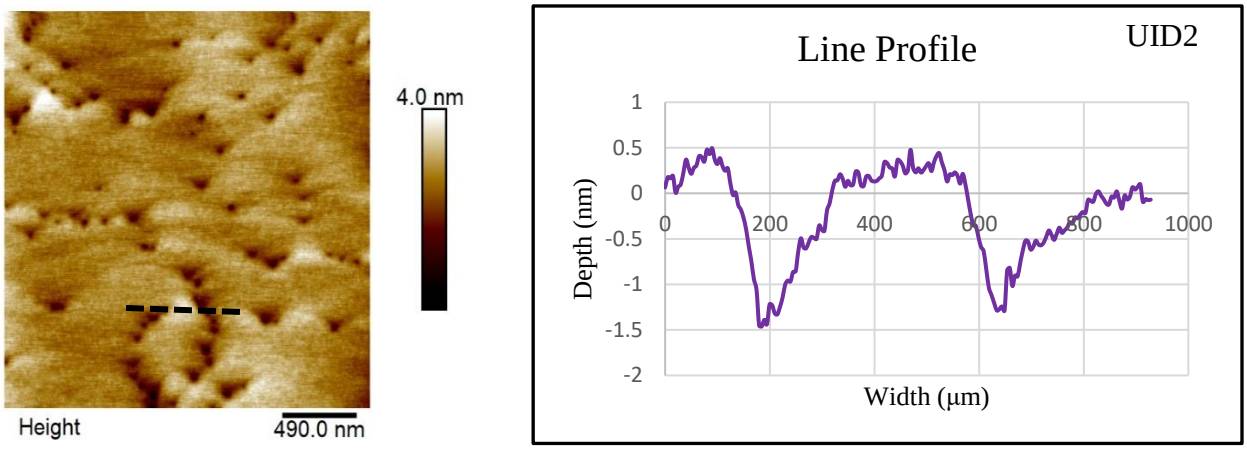

Figure 31. Pits distributed randomly in UID2 with different depths and widths. The line profile is through the drawn line in AFM image at the left.

UID2 substrate. The measurement was done on the substrate to compare the AFM images with SEM images and calculate the defect density on the surface of UID2 substrate. Figure 32 shows the shape of the pits on the surface which were hexagonal V-shape pits. The number of hexagonal V-shape pits was lower than UID1, and they were distributed randomly on the surface of UID2 substrate with different size. The size of the hexagonal V-shape pits ranged from 30 nm to 400 nm in diameter (Figure 32).

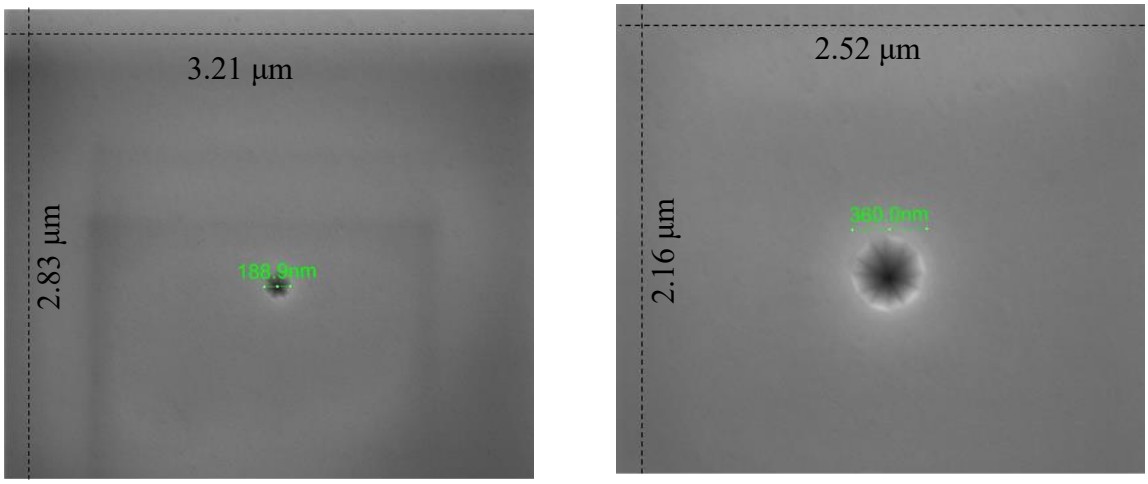

Figure 32. SEM images showing the size of V-shape pits in UID2.

The hexagonal V-shape pit density was very low, and many places seemed to be almost clear of them (Figure33). To calculate the size distribution and density of the hexagonal V-shape pits, mapping the surface of UID2 was carried out. The size of the images was 8.28 × 6.48 μm. The defect density of the hexagonal V-shape pits was estimated to be approximately 1.6×10^{5} cm^{-2}. The formation of the V-shape pits was due to the threading dislocation densities in the structure of UID2.

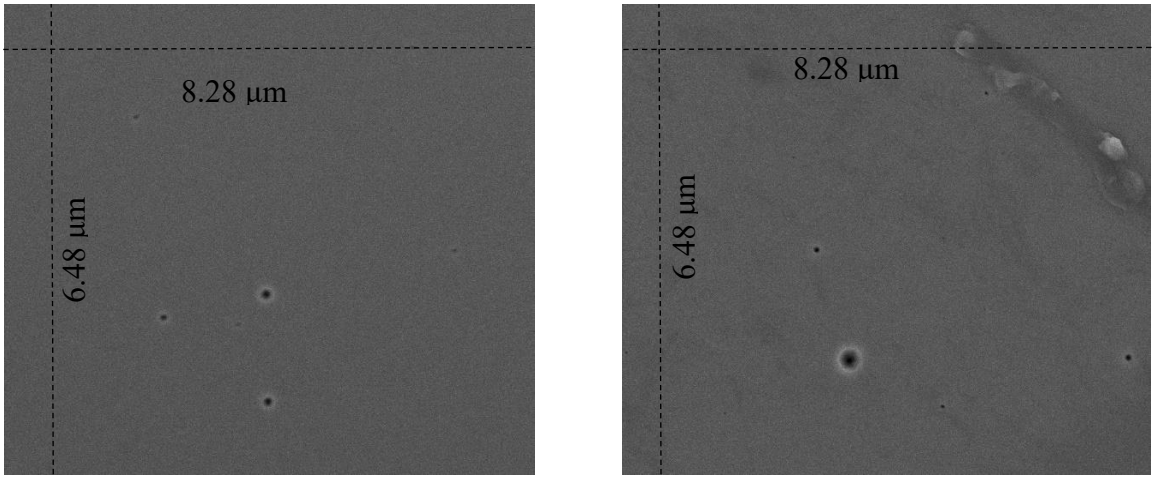

Figure 33. SEM images showing lower pit density in UID2.

Optical Microscope

In addition to AFM and SEM measurements to investigate the surface morphology of the UID2 substrate, optical microscopy was performed to analyze more defects in UID2 surface. Optical microscopy is an important technique to study material surfaces at a large scale. By optical microscope, the surface seemed clear of any big defects as seen in UID1 (bumps). Mapping the surface and using different magnification to detect defects were applied on UID2. However, as shown in Figure 34, the surface had almost no defects. It is suspected that the same features as seen in the UID1 substrate, Figure 20, were present, because the same large features were present in the AFM (compare Figure 16 and Figure 27). However, due to the uncoated backside, UID2 did not show the contrast due to these features in the optical microscope.

Figure 34. Optical microscope images for UID2 showing that the surface does not suffer from big terraces as UID1.

In summary, the morphology of the UID2 substrate was studied by three different types of microscopy. AFM measurements were carried out to characterize the surface morphology. The surface contained some micro-pits. The total micro-pit density was 8.9×10^{8} cm^{-2}. Mapping

by SEM was performed to study the defect density in UID2 substrate. Hexagonal V-shape pits were noticed by SEM. The hexagonal V-shape pits had different size spreading in the surface. The total V-shape pit density was 1.6×10^5 cm^{-2}. Optical microscopy was used to study the surface over a large scale. UID2 surface looked clear from macro-defects, however, it is suspected that this was only due to the lack of contrast provided by the Ti backside coating.

3.2.2 Structure Characterization

X-Ray Diffraction

In order to investigate the UID2 structure, XRD rocking curve ω-scans were measured to study the quality of the material and the dislocation densities. The rocking curve ω-scan was performed on the (002) symmetric reflection (Figure 35) and the (102) asymmetric reflection (Figure 36). The full width at half maximum (FWHM) values for (002) and (102) reflections were 296 arcsec and 531 arcsec, respectively. The FWHM is associated with lattice distortion, so the threading dislocations can be calculated by using FWHM values. The FWHM value for (002) is related to the screw dislocation density, and FWHM value for (102) is associated with the mixed dislocation density including screw and edge dislocations. The screw dislocation density of (002) reflection was 1.73×10^8 cm^{-2}. The mixed dislocation density of (102) reflection was 1.48×10^9 cm^{-2}. In comparison with UID1, UID2 had much lower dislocation density. This is believed to be due to normal variation from the manufacturer.

Optical Transmission

Optical transmission is a measurement to study the optical quality of materials. Transmission was used to investigate the variety of transmitted radiation for a series of wavelengths. A spectrometer with deuterium and tungsten lamps was used. These light sources

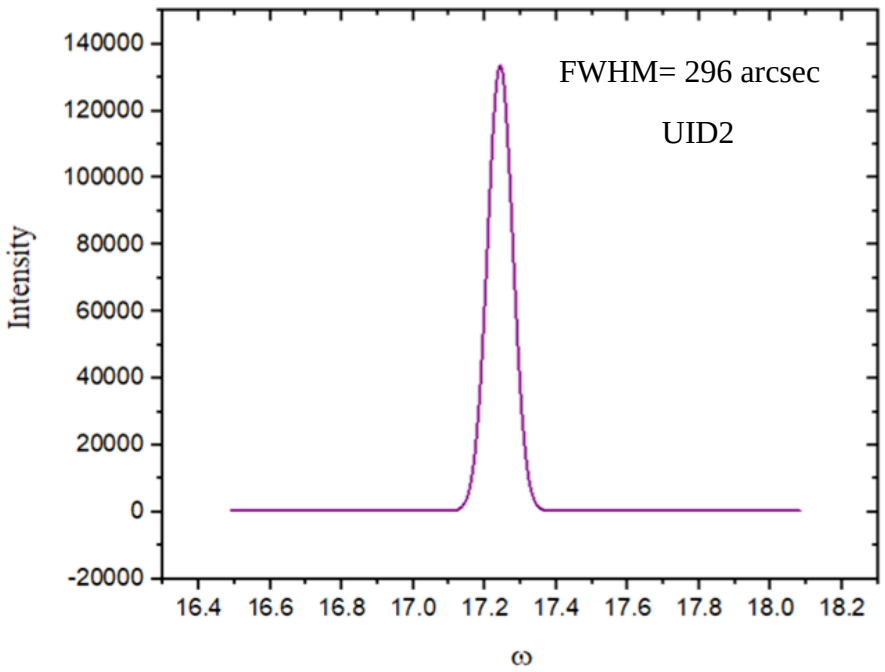

Figure 35. X-ray peak associated with screw dislocations from (002) reflections for UID2.

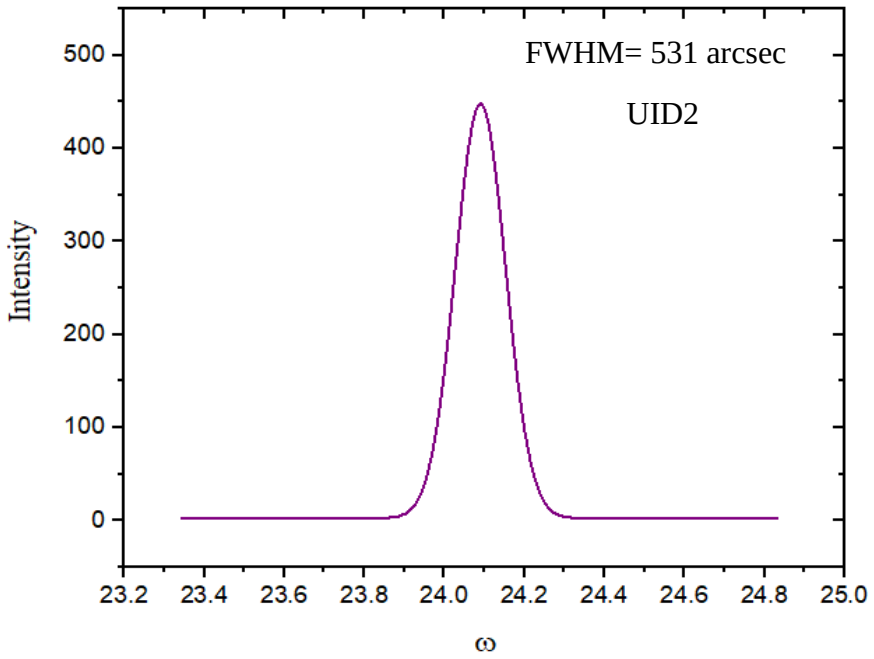

Figure 36. X-ray peak associated with mixed dislocations from (102) reflections for UID2.

produce a large range of wavelengths from 200 to 1700 nm to determine the material bandgap. The optical transmission measurement was done at room temperature. A typical transmission measurement is shown in Figure 37. The transmission of air was used as a reference for UID2, the backside of UID2 has a rough texture. For these reasons, the absolute values for the transmittance were not accurate. However, as shown in Figure 37, when the incident radiation had energy equal to or larger than the bandgap energy, it was absorbed strongly in UID2, i.e., the transmittance vanished. On the other hand, radiation with energy less than the bandgap energy was transmitted. Therefore, the turn-on point denotes the bandgap energy.

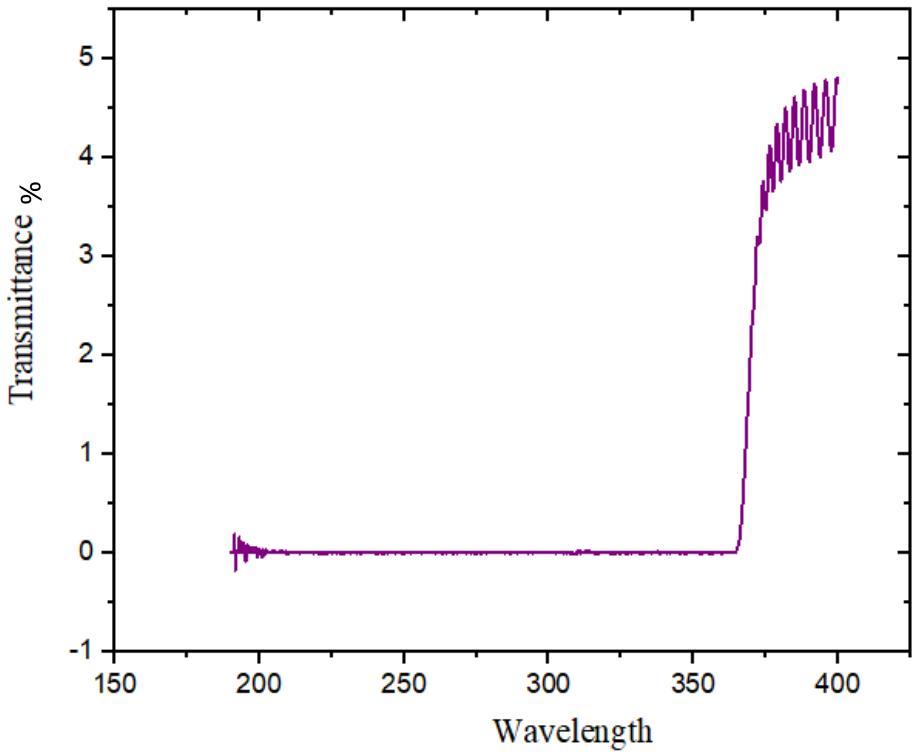

Figure 37. Optical transmission measurement to determine UID2 bandgap.

The transmission was calculated by using the reference energy (air) (I_0) and UID energy (I). Equation 6 was used to calculate the percentage of transmission.

$$T = \frac{I}{I_0} \times 100 \qquad \text{(Equation 6)}$$

From Figure 37, the bandgap energy was 3.39 eV which is the typical value for GaN bandgap at room temperature. This indicates that the optical properties of UID2 were not affected by the defects in the structure and the surface.

3.3 Semi-Insulating GaN on Sapphire with Titanium

A semi-insulating (SI) HVPE GaN on sapphire (SI1) substrate with Ti was investigated by several microscopy techniques for the surface and optical characterization of the structure quality. SI1 was doped with iron (Fe) at approximately 1×10^{18} cm^{-3}. SI1 was a 2-inch diameter wafer with and 5 μm of SI GaN was grown on the polished side. The surface morphology was characterized by AFM, optical microscope, and SEM measurements. The quality of the structure was characterized by x-ray diffraction, and optical characterization (PL and CL) was done on the SI1 substrate.

3.3.1 Morphology Characterization

Atomic Force Microscopy

AFM is an essential technique in this research to characterize the surface quality, roughness, and the various defect densities on the substrate. The characterization was by using a silicon tip with a small radius of curvature of approximately 10 nm. The surface of SI1 was investigated in many different places to observe the defects and study the uniformity of the surface. AFM measurements showed that the surface was clear of the hexagonal pits and distorted pits. Even though, Figure 38 shows a relatively smooth AFM image for SI1, it shows that the surface contained a new form of defect in the form of large hillocks. These hillocks were

9 to 10 nm in height and 3 to 5 µm in width. It has been shown that many features similar to these hillocks are also associated with the termination of dislocations [30], [53]. The roughness of this area was around 2.24 nm. Moreover, the SI1 surface contained some distorted hillocks (Figure 39). The height of these bumps ranged from 4 to 6 nm, and the width from 3 to 4 µm. The roughness value of the surface was 1.68 nm.

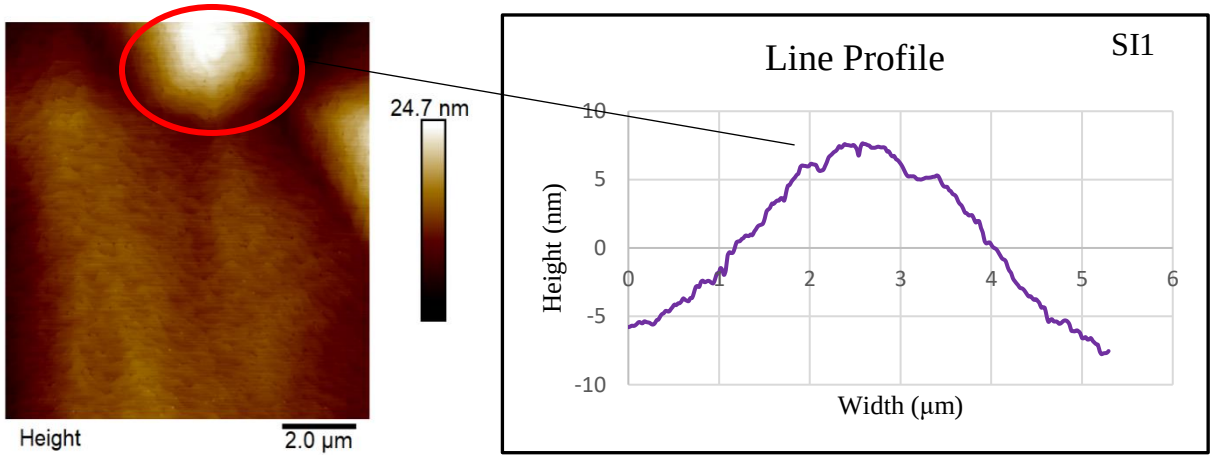

Figure 38. AFM image showing that SI1 has hillocks with height 8 nm. The line profile is through the red circle in the AFM image at left.

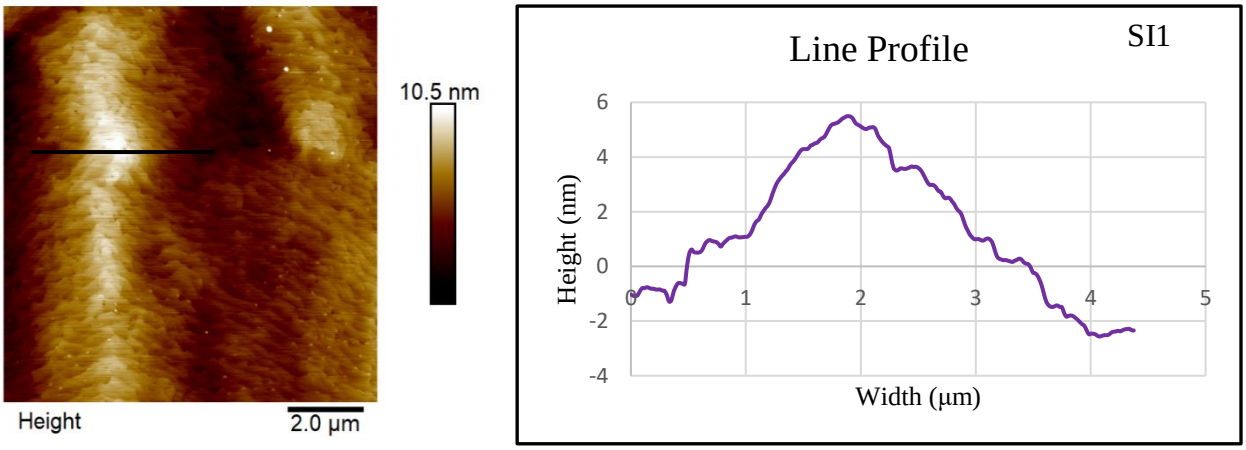

Figure 39. AFM image showing that SI1 has bumps that can be extended from hillocks with height 5 nm. The line profile is through the line drawn in the AFM image at left.

Scanning Electron Microscope

In addition to AFM measurements, SEM images were obtained on SI1 substrate. The measurement was done on the substrate to compare the AFM images with SEM images and calculate the defect density on the surface of SI1 substrate. However, new defects were observed by SEM which were not evident in either of the UID substrates. These defects were big pits (macro-pits) which ranged from 100 μm to 300μm in diameter. Figure 40 shows the shape of the macro-pits on the surface which was hexagonal with a hole in the center. These macro-pits indicated that the structure of the SI1 suffered from threading dislocations that appeared as an aperture surrounded by a macro-pit.

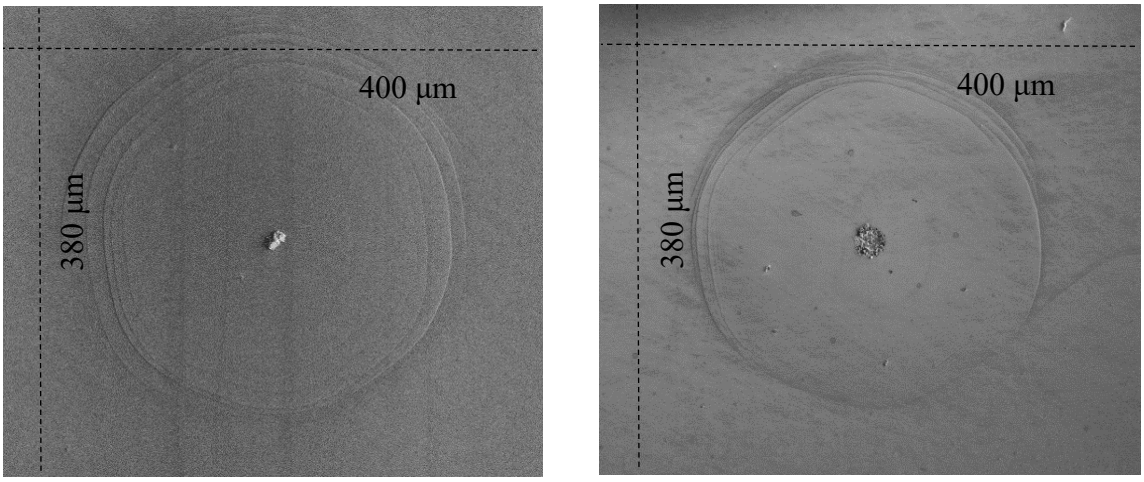

Figure 40. SEM images for macro-scale pits with small aperture in the middle in SI1.

Optical Microscope

Since SI1 contained macro-pits, optical microscope was a critical technique to study the surface over a wide range and do mapping to calculate the density of the macro-pits. The macro-pits had different sizes ranging from 100 μm to 300 μm. Some of these macro-pits were found to overlap with each other, and some macro-pits contained from two to three apertures in the center

which indicate that there are two or three dislocations in the same macro-pit (Figure 41). These macro-pits were spread randomly over the surface. The total macro-pits density was approximately 2.49×10^2 cm^{-2}.

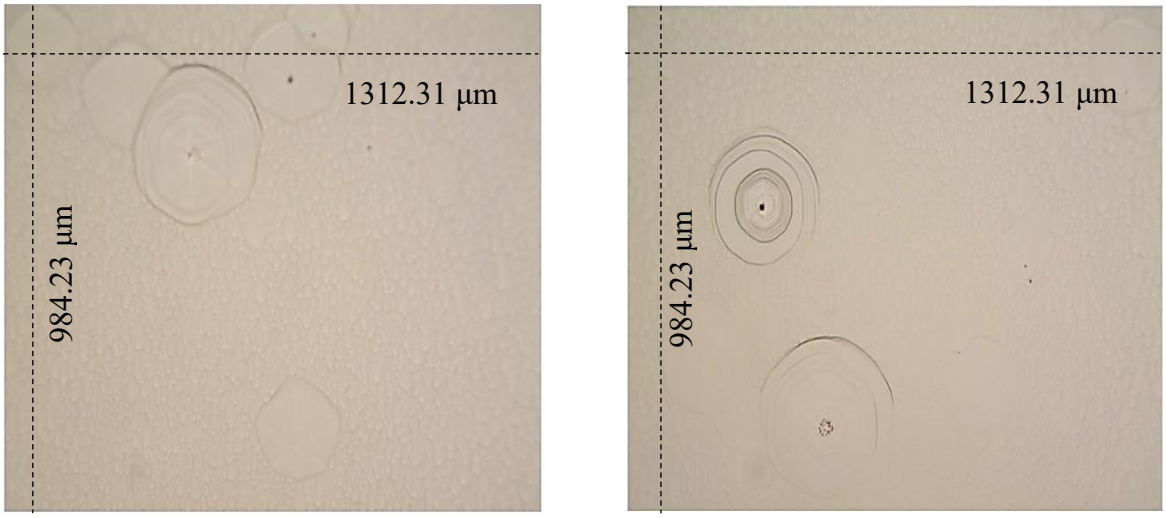

Figure 41. Optical microscope images showing the same results as SEM–macro-scale pits with small aperture in the middle in SI1.

In summary, the morphology of SI1 substrate was studied by three different types of microscope. AFM measurements were carried out to characterize the surface morphology. The surface contained some hillocks. The surface did not have any small pits as shown by AFM images. SEM was performed to study the defects in SI1 substrate. Macro-pits were observed by SEM. Macro-pits had different sizes spread around the surface. Optical microscopy was used to study the surface over a large scale and to calculate the macro-pit density in the surface. The total macro-pit density was calculated to be approximately 2.49×10^2 cm^{-2}.

3.3.2 Structure Characterization

X-Ray Diffraction

In order to investigate SI1 structure, high resolution x-ray diffraction was performed. The rocking curve ω-scan was essential to measure the quality of the material, detecting the dislocation density and sample curvature. The rocking curve ω-scan was performed to study (002) symmetric (Figure 42) and (102) asymmetric reflections (Figure 43). The full width at half maximum (FWHM) values for (002) and (102) reflections were 273 arcsec and 507 arcsec, respectively. The FWHM value for (002) is related to the screw dislocation density, and FWHM value for (102) is associated with the mixed dislocation density including screw dislocations and edge dislocations. The screw dislocation density of (002) reflection was 1.48×10^{8} cm^{-2}. The mixed dislocation density of (102) reflection was 1.34×10^{9} cm^{-2}.

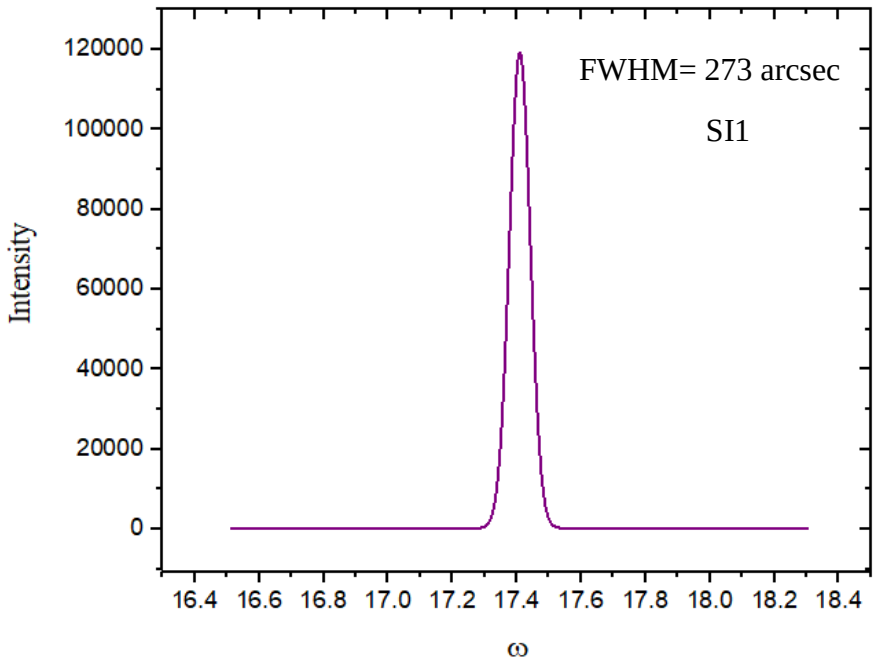

Figure 42. Rocking curve for symmetric (002) reflections associated with screw dislocation for SI1

Cathodoluminescence

Cathodoluminescence (CL) is an important technique to study the effect of defects on

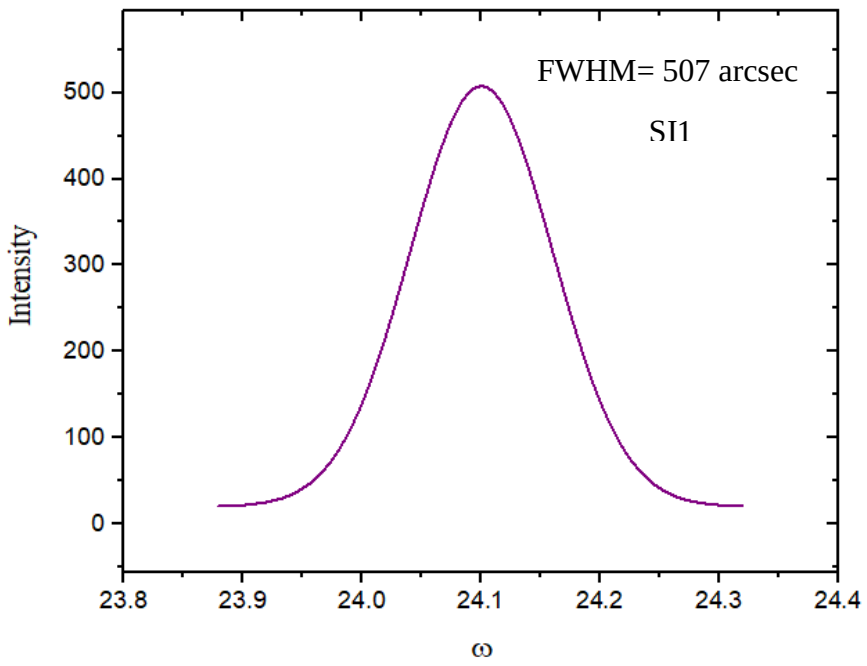

Figure 43. Rocking curve of asymmetric (102) reflections associated with mixed dislocation for SI1

the optical properties of GaN substrates. Therefore, CL measurements were performed on SI1 to investigate the holes in the substrate and their effects. Measurements were taken inside the holes and outside the holes to investigate the change in the SI1 substrate optical properties and how those properties were affected by the structural and surface defects in the substrate. In this measurement, the electron beam energy was 10 KeV, the measurements were at a low temperature of ~ 90 K, and the scanning areas ranged from 200 μm to 300 μm depending on the hole size. Figure 44 illustrates two results of CL measurements in the first hole. Figure 44a is a panchromatic CL image for the characterized hole. The panchromatic image was obtained by collecting the undispersed light emitted from each point in the image area. The center of the big hole was the center of the dislocation that propagated from within the substrate to the surface and appeared as an aperture. Figure 44b illustrates the CL spectrum inside the hole with two visible peaks. The wavelength of highest energy peak was ~360 nm which is the near band edge

emission (NBE) of GaN. The energy of NBE is ~3.4 eV. Then, the very broad middle energy peak, which had a maximum at 439 nm is generally called the blue luminescence band (BL), and its energy is 2.8 eV [54]. Generally, BL is associated with point defects such as Ga vacancies [55], [49]. Figure 44c shows the CL spectrum outside the hole. Also, there were two luminescence peaks which were NBE and BL. However, the intensity outside the hole was lower than the intensity inside the hole which correlates with the panchromatic image being more intense there.

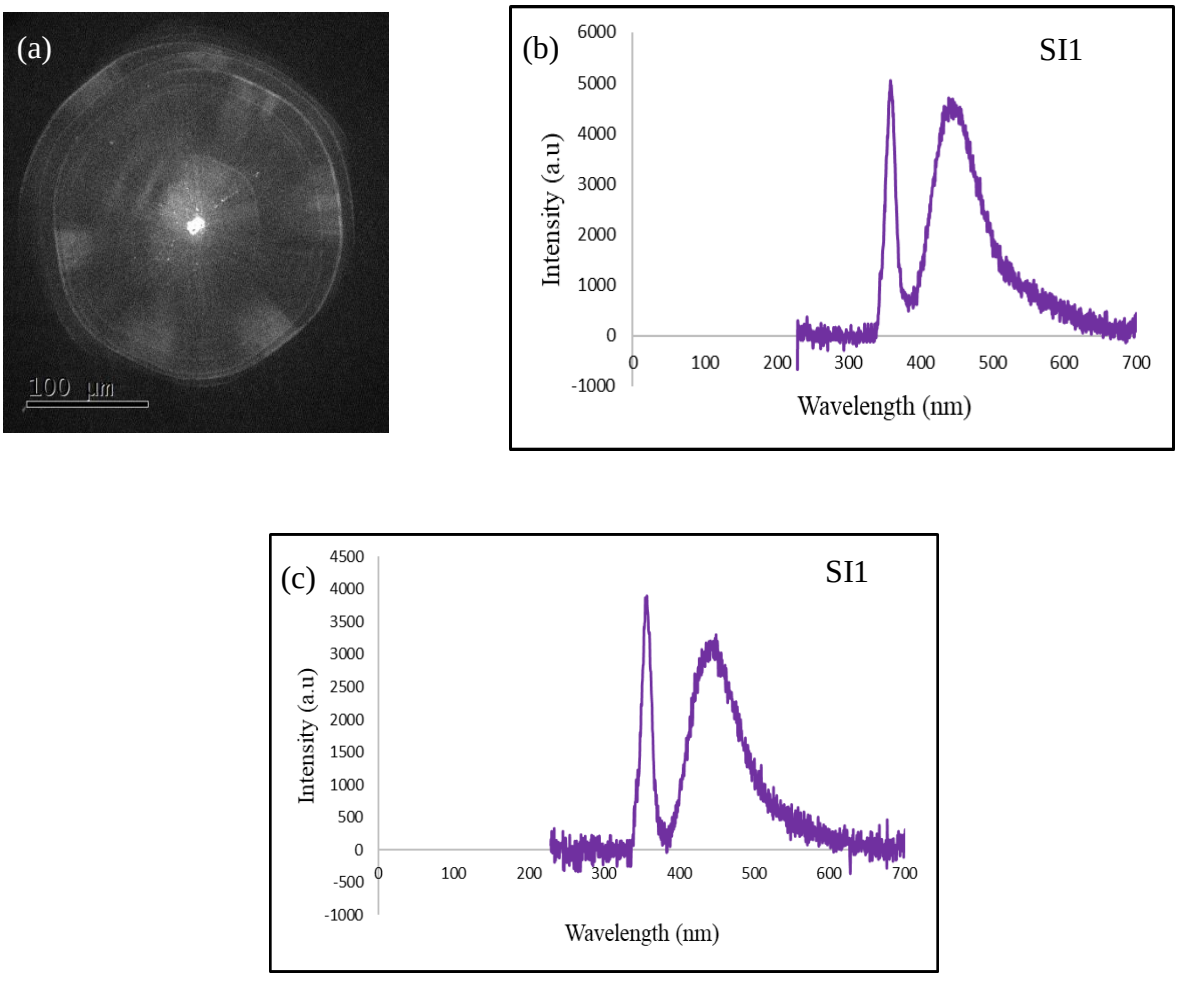

Figure 44. CL measurements for SI1: (a) panchromatic image for the hole, (b) CL spectrum inside the hole showing GaN peak and blue band peak, and (c) CL spectrum outside the hole showing GAN peak and blue band peaks with lower intensity.

A second hole was measured by CL resulting in slightly different results. As shown in Figure 45a, the panchromatic image shows a bright spot in the middle similar to the first hole. Figure 45b illustrates the CL spectrum. Here, there appears to be one extra peak as compared with the first hole. NBE was observed at 3.4 eV. BL was detected at 2.8 eV [56]. The new peak observed close to the NBE was at 371 nm or 3.34 eV. This luminescence is commonly known as the violet luminescence band (VB). VB occurs around dislocations with high intensity. Therefore, the dislocation in the structure can be the origin of VB. Also, the point defect or radiative defects were associated with the existing VB. In contrast, Figure 45c illustrates the CL spectrum outside the hole with only two peaks, the NBE and the BL. This reinforces the idea that the VB was directly due to the threading dislocation at the core of the hole.

A third hole was measured by CL with slightly different results. Similar to before, Figure 46a shows the panchromatic image for the third hole. Figure 46b illustrates the CL spectrum. Here, there appeared four distinct peaks. In addition to the NBE, BL, and VB, there appeared a new peak at ~2.2 eV or 558 nm. This luminescence is commonly known as the yellow luminescence band (YB) [56], [57]. YB can be associated with the point defects such as a Ga vacancy [58]. Also, it can occur around a dislocation. Figure 47 shows a scheme of transitions across the bandgap including several optically active trap states which are possibilities to explain the luminescent bands. These are presented for reference but will not be discussed further as they are outside the scope of this thesis.

3.3.3 Growth 1 µm of GaN on SI1

Many characterizations methods were performed on SI1 substrate, and different structural and morphological defects were found on SI1 substrate. Therefore, to know if those defects affected the subsequent growth and, then, the performance of the subsequent devices, SI1 was

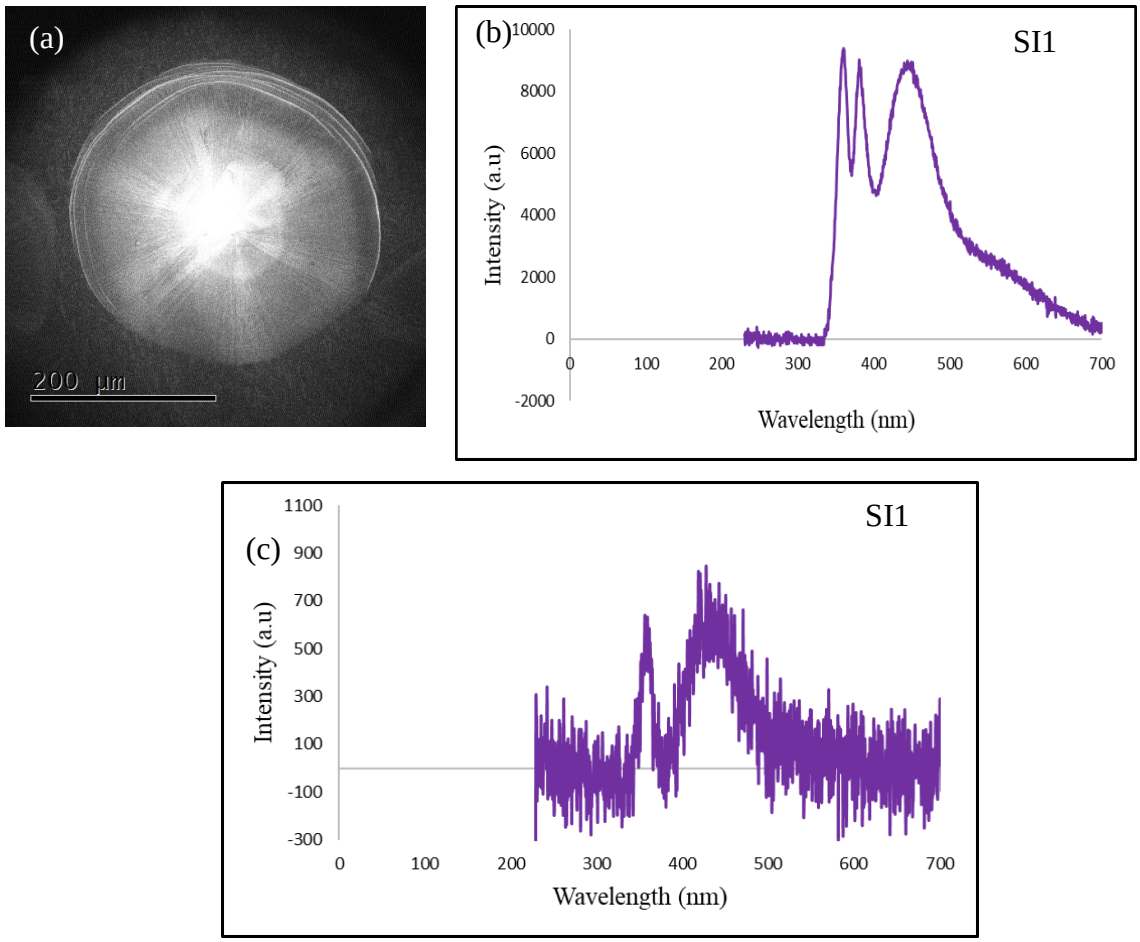

Figure 45. CL measurements for SI1: (a) panchromatic image for the hole, (b) CL spectrum inside the hole showing GaN peak, violet and blue band peaks, and (c) CL spectrum outside the hole showing GAN and blue band peaks with lower intensity.

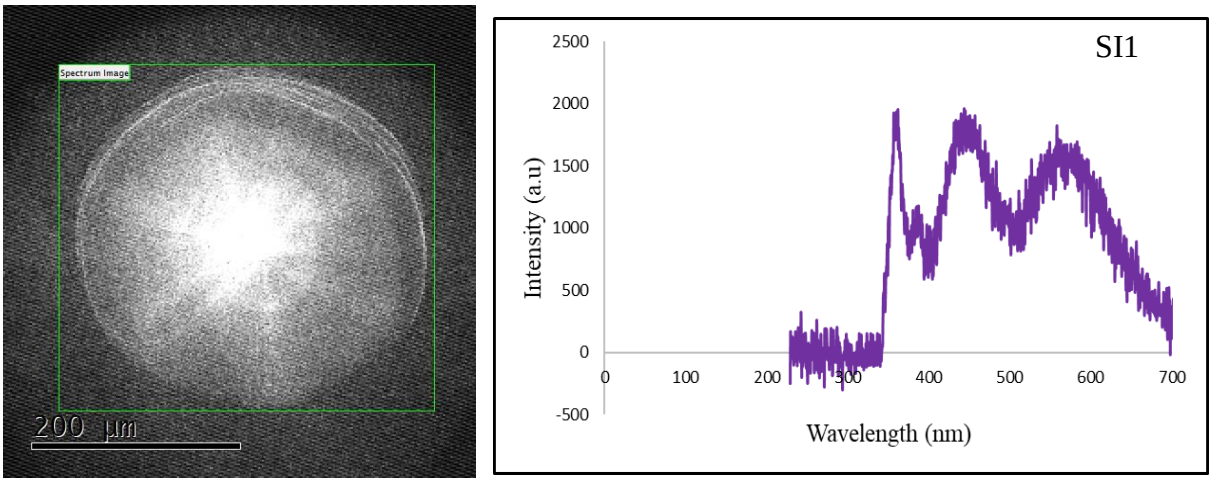

Figure 46. CL measurements for SI1: (a) panchromatic image for the hole and (b) CL spectrum inside the hole showing GaN peak and violet, yellow, and blue band peaks.

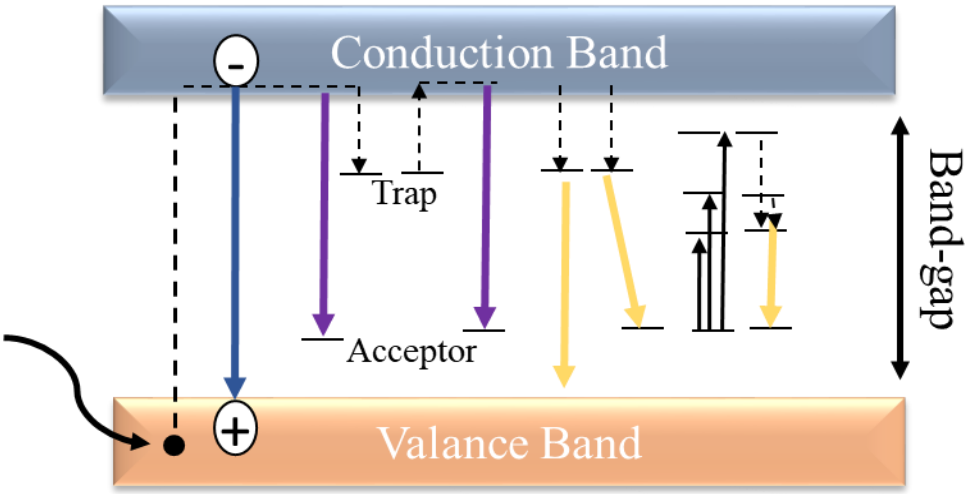

Figure 47. Schematic of the exciton electron and illustration of the formation of luminescence peak.

cut to four quarters in order to grow GaN layer on one quarter section. GaN was then grown to a thickness of 1 μm by molecular beam epitaxy (MBE) at 800 °C. This growth was then characterized by AFM.

Atomic Force Microscopy

The surface of the GaN on SI1 substrate was mapped by AFM to investigate the whole sample and detect the defects that existed in both the substrate and GaN layer. The defect density was then counted for 10 × 10 μm images. Many defects were detected on the GaN on SI1 substrate. The surface suffered from hillocks with height ranging from 4 to 8 nm and width ranging from 3 to 5 μm (Figure 48). The roughness of those areas varied from 1.60 and 2.04 nm. More defects were observed after the growth. Figure 49 showed that this area contained some micro-pits with a pit density of 5.45×10^{8} cm^{-2}, but the area had a smooth surface with 0.79 nm of roughness. However, in some areas, there were distorted pits and cracks with lengths varying from 0.6 to 2.79 μm. The depth of those cracks was approximately 10 nm, and the roughness value was 3.34 nm (Figure 50).

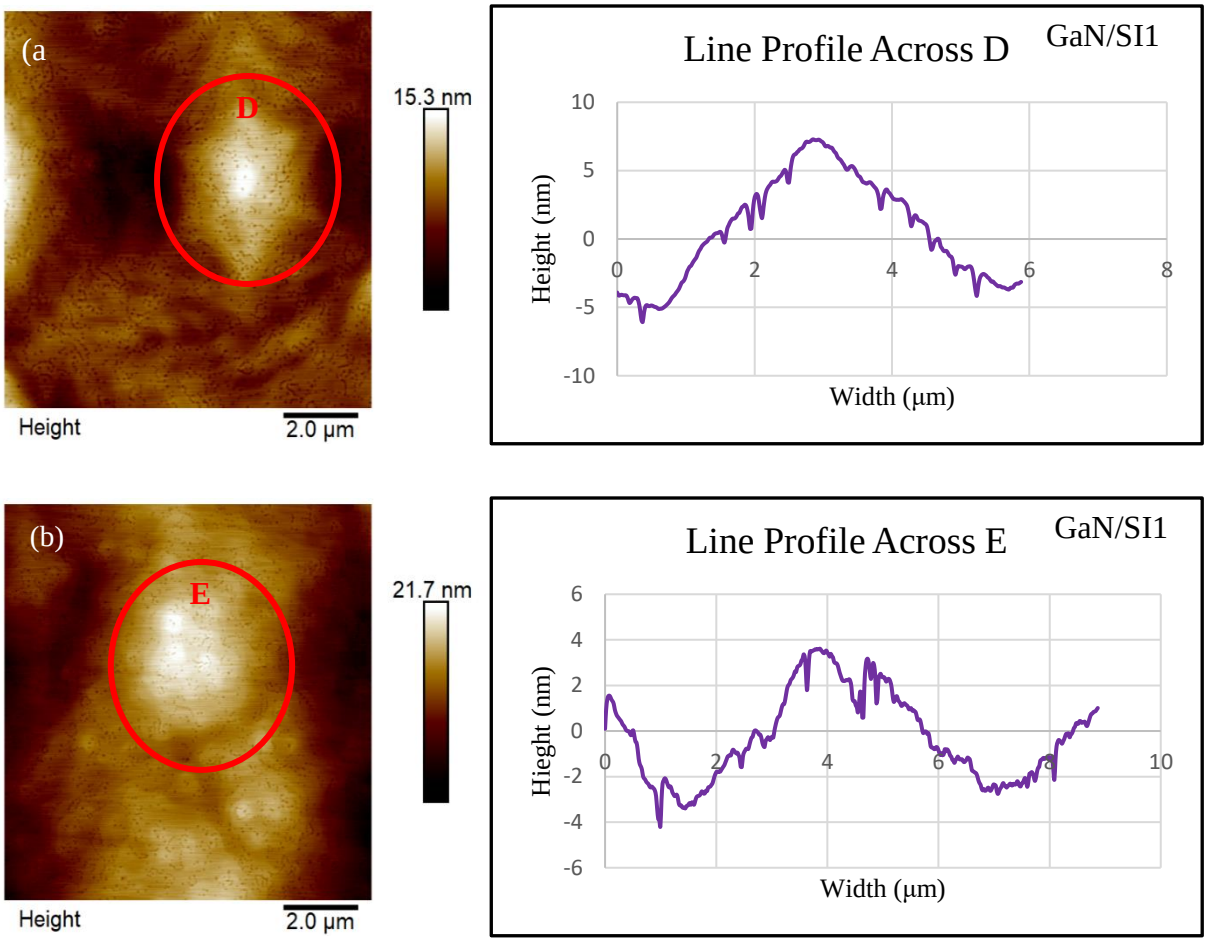

Figure 48. AFM images for GaN buffer layer on SI1: D) hillocks and E) distorted hillocks.

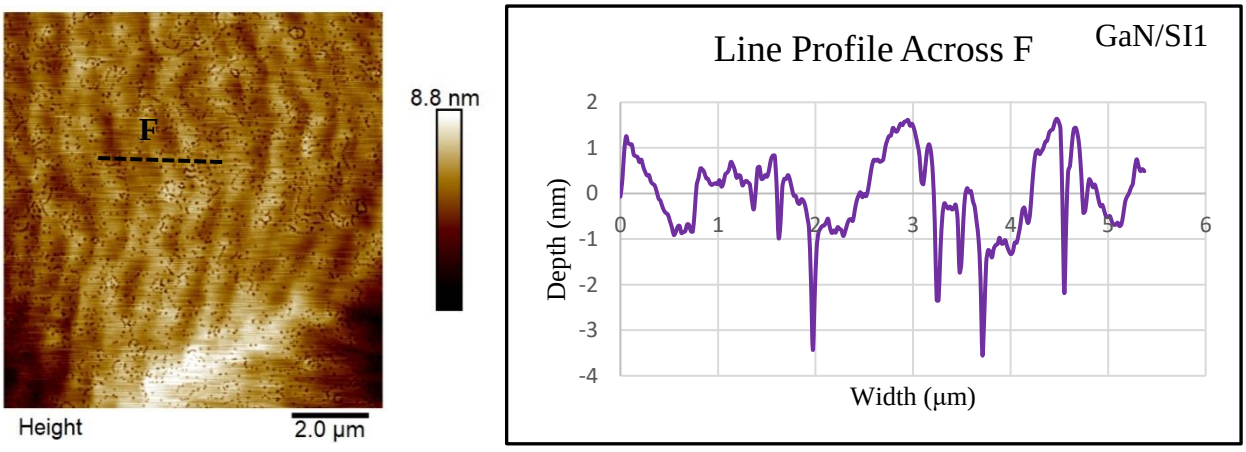

Figure 49. AFM image showing small pit density on SI1 after GaN buffer layer growth.

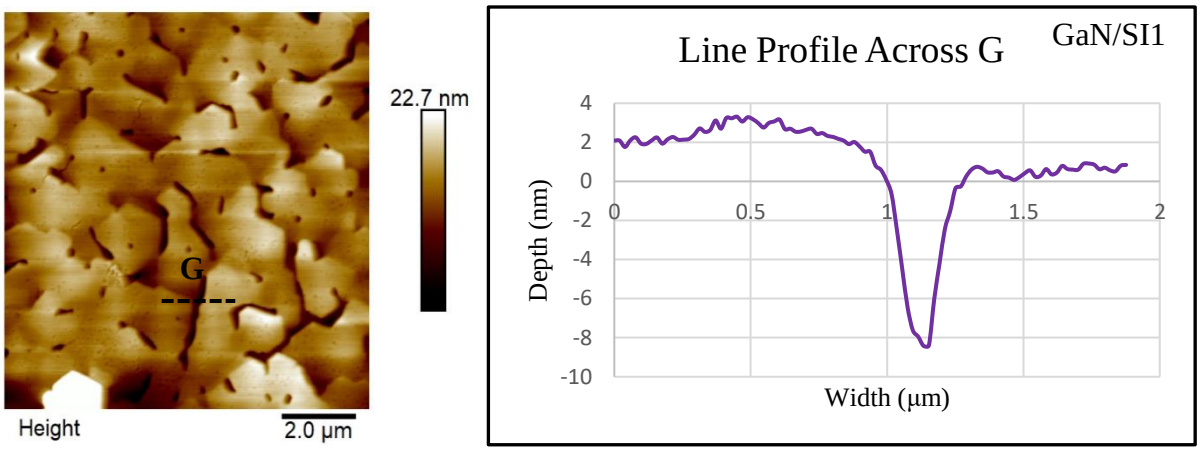

Figure 50. AFM images of SI1 showing small pits and cracks in the surface after growth. The line profile is through G line to show the depth of the crack.

3.4 Semi-Insulating GaN on Sapphire with no Titanium

The second semi-insulating, HVPE grown GaN on sapphire substrate (SI2) had no Ti backside coating and was investigated by several microscopy techniques for the surface and optical characterization of the structure quality. Similar to SI1, SI2 was a 2-inch sapphire wafer with 5 µm of GaN grown on the polished side and doped with iron (Fe) at a concentration of ~1 × 10^{18} cm^{-3}. The surface morphology was characterized by AFM and optical microscopy, and the quality of the structure was characterized by x-ray diffraction and optical transmission.

3.4.1 Morphology Characterization

Atomic Force Microscopy

AFM characterization was performed using a silicon tip with a small radius of curvature of approximately 10 nm. The surface of SI2 was investigated in many different places to detect the defects. The SI2 surface was almost clear from the hexagonal pits and distorted pits as AFM measurements show. Figure 51 shows a representative smooth AFM image for SI2 with only some small hillocks. Those hillocks were 9 to 10 nm in height and 3 to 5 µm in width and were

generally understood, similar to before, to be associated with the termination of dislocations. The roughness of this area was around 4.25 nm. Similar to SI1, the SI2 surface contained some bumps (Figure 52). The height of those bumps ranged from 4 nm to 6 nm, and the width ranged from 4 to 9 µm. The roughness value of the surface was 2.81 nm.

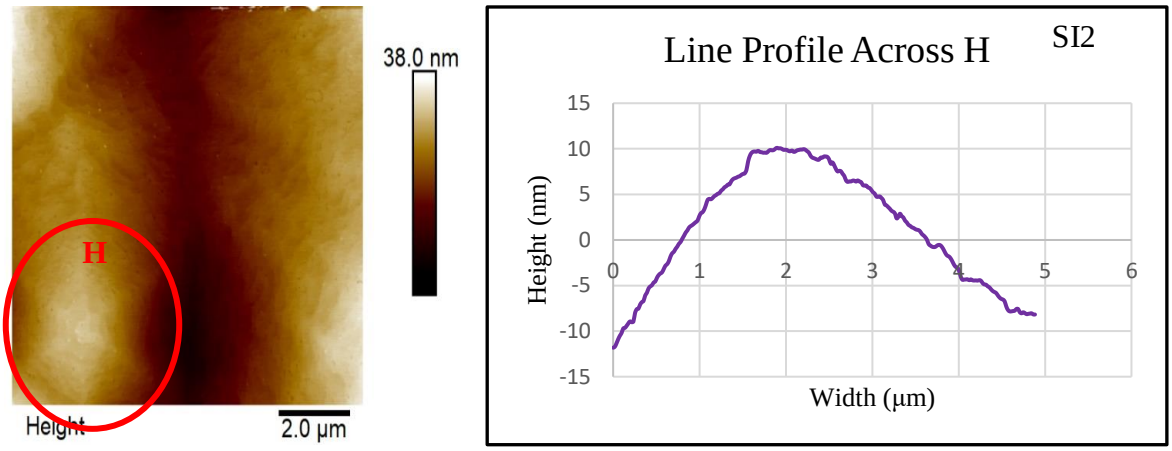

Figure 51. AFM image showing that SI2 had some hillocks with height 10 nm.

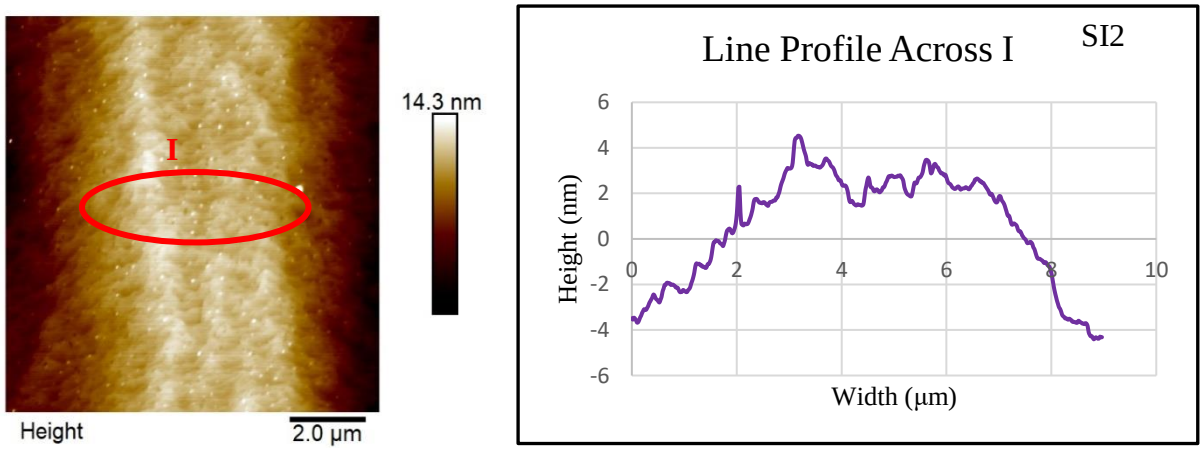

Figure 52. AFM image showing that SI2 had some bumps that can be extended from hillocks with height 4 nm.

Optical Microcopy

Similar to SI1, SI2 still contained large scale macro-pits. Therefore, an optical microscope was used to study the surface over a large scale. Also, to compare with SI1, mapping the surface and calculating the density of the macro-pits were done. By optical microscope, mapping was carried out over an image with dimensions of 1258 μm × 915.3 μm. Macro-pits had different sizes ranging from 100 μm to 300 μm. Some of these macro-pits overlapped with each other as shown in Figure 53, and some macro-pits contained from two to three apertures in the center due to two or three dislocations in the same macro-pit (Figure 53). The macro-pits were spread randomly on the surface. The total macro-pits density was approximately 5×10^2 cm^{-2}, which was very similar to SI1.

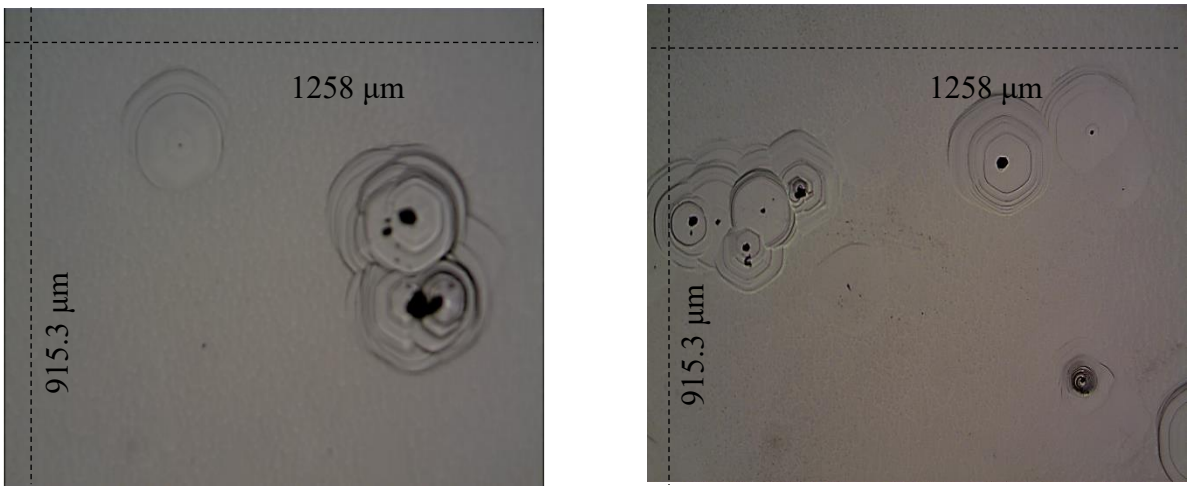

Figure 53. Optical microscope images to illustrate the size and shape of macro-scale pits in SI2.

In summary, the morphology of the SI2 substrate was studied by two different types of microscope. AFM measurements were carried out to characterize the surface morphology. The surface contained some hillocks. The surface did not have any pits as shown in AFM images. Macro-pits were detected by optical microscope, and they had different sizes randomly distributed across the surface, with an average density of ~5×10^2 cm^{-2}.

3.4.2 Structure Characterization

X-Ray Diffraction

In order to investigate the SI2 structure, many different characterization tests were performed. High resolution x-ray diffraction was a critical technique to study the structure of the SI2 substrate. The rocking curve ω-scan was essential to measure the quality of the material and detect the dislocation density. The rocking curve ω-scan was performed to study (002) symmetric (Figure 54) and (102) asymmetric reflections (Figure 55). The full width at half maximum (FWHM) values for (002) and (102) reflections were 307 arcsec and 504 arcsec, respectively. The FWHM value for (002) is related to the screw dislocation density, and FWHM value for (102) is associated with the mixed dislocation density including screw dislocation and edge dislocation. The screw dislocation density of (002) reflection was 1.88×10^8 cm^{-2}. The mixed dislocation density of (102) reflection was 1.33×10^9 cm^{-2}.

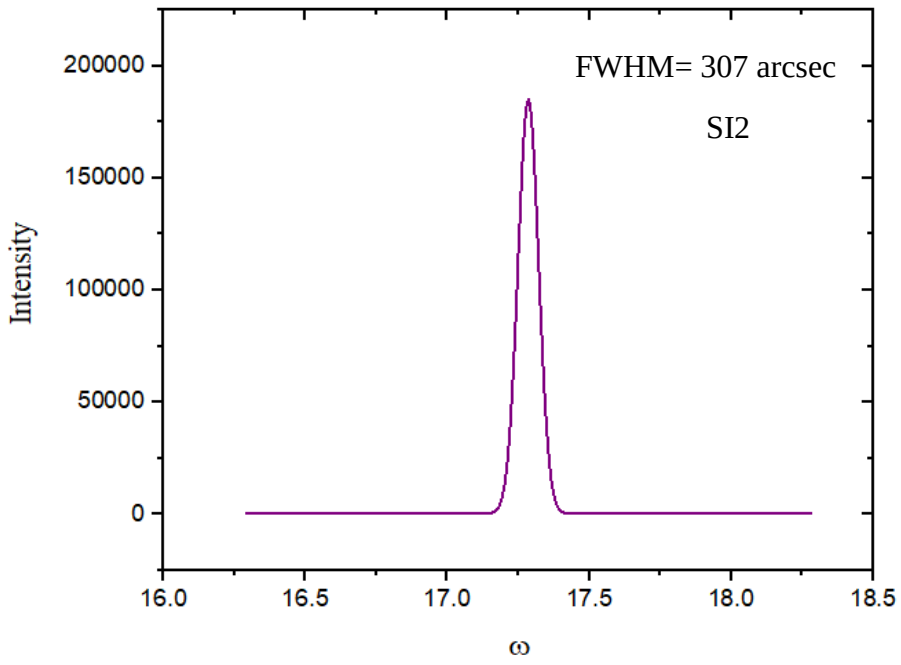

Figure 54. XRD rocking curve of symmetric (002) reflections associated with screw dislocations for SI2.

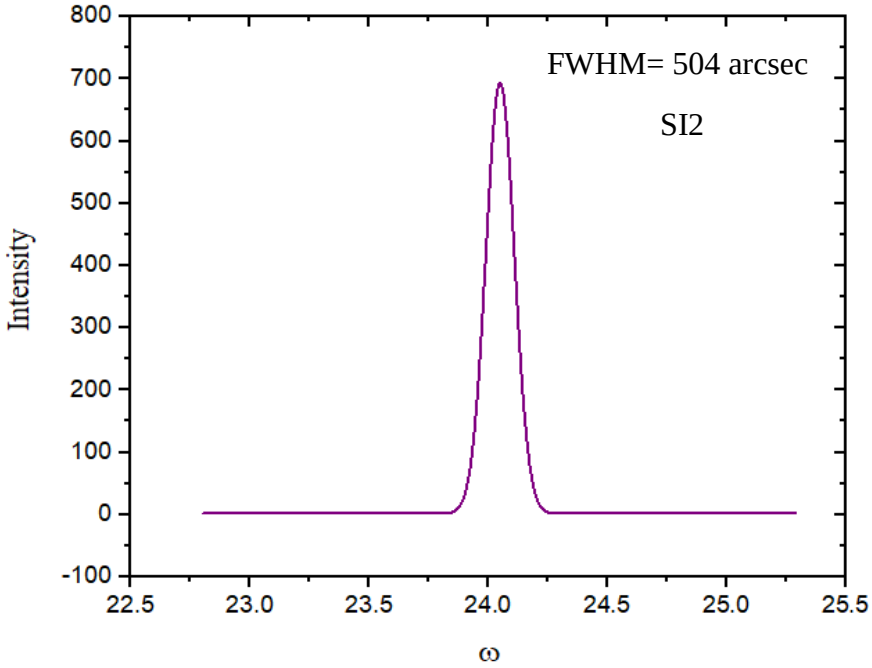

Figure 55. XRD rocking curve of asymmetric (102) reflections associated with mixed dislocations for SI2.

Optical Transmission

Optical transmission is a measurement to study the optical quality of materials. Transmission was used to generally investigate the optical bandgap of the substrate at room temperature. A typical transmission measurement is shown in Figure 56. As shown in Figure 56, light with energy equal to or larger than the bandgap energy was strongly absorbed, however, light with energy smaller than the bandgap energy was transmitted. The transmission was calculated by the using the reference energy (air) (I_0) and SI2 energy (I) in Equation 6. From Figure 56, the bandgap energy was 3.4 eV which is, similar to before, the typical value for GaN bandgap at room temperature. This indicates that the optical properties of SI2 were not affected by the defects in the structure and surface.

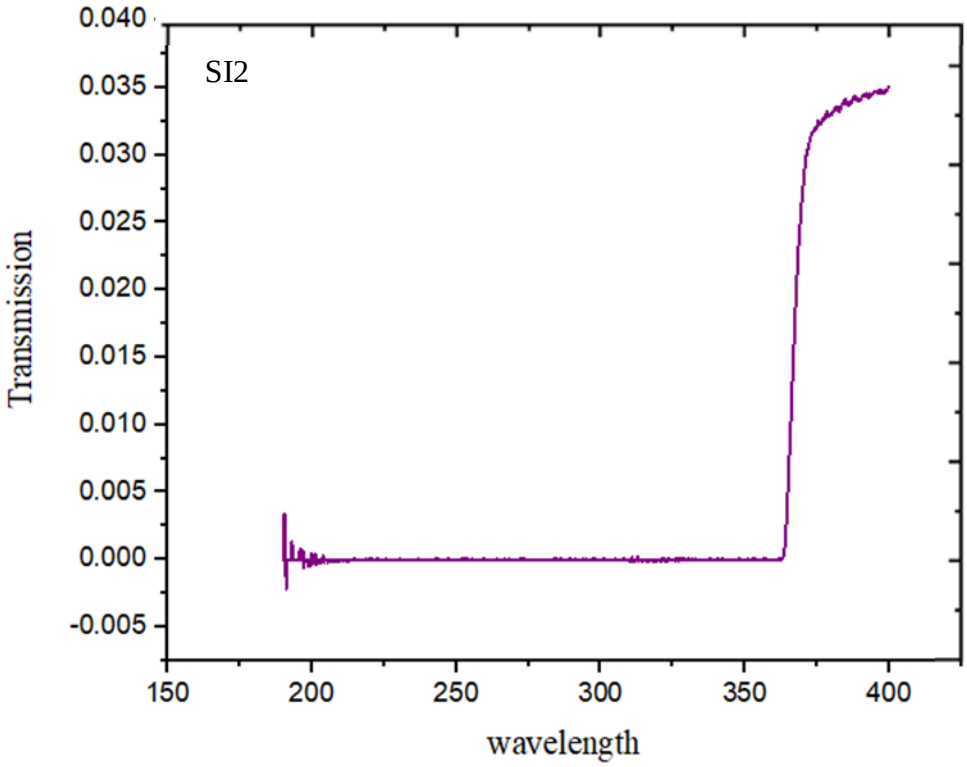

Figure 56. Optical transmission for SI2 to determine the bandgap.

Chapter 4: Conclusion and Future Work

The quality of commercially obtained gallium nitride (GaN) on sapphire substrates that have been grown by using hydride vaper phase epitaxy (HVPE) was investigated and characterized in this work. Several techniques were employed to investigate the GaN substrates because they are the best choice for optoelectronic applications due to their physical and electrical properties. Four GaN substrates were characterized by atomic force microscopy (AFM), optical microscopy, and scanning electron microscopy (TEM) to study the surface morphology. Furthermore, the structural and optical properties were characterized by x-ray diffraction (XRD), cathodoluminescence (CL), and optical transmission. From these characterizations, it was found that the substrates suffered from large macro-scale defects in the surface that were the result of the defects in the structure. Subsequently, 1 μm of GaN was grown using two of the substrates to investigate the effect of those defects on the subsequent growth. The investigations were performed by AFM and transmission electron microscopy (TEM).

The morphology investigations were performed on two unintentionally doped GaN on sapphire substrates (UID1 & UID2) and two semi-insulating GaN on sapphire substrates (SI1 & SI2). AFM measurements were carried out to characterize the surface morphology of UID1 and UID2. Four types of defects were observed by AFM which were small pits, big pits, large terraces and ridges on the surface of UID1. After mapping the UID1 substrate surface, the small pit density was calculated to be approximately 10^8 cm^{-2}, and the big pits were around 10^6 cm^{-2}. Even though UID2 had approximately the same number of pits, about 10^8 cm^{-2}, the size and the depth of the pits were smaller than that existing in UID1. Also, the terraces in UID1 were larger than those in UID2; the step height of the terraces in UID1 was around 90 nm and in UID2 was around 30 nm. SEM measurements showed the pit density on both UID1 and UID2, but the pit

density in UID2 was much lower than that in UID1. The pit density in UID1 was 10^7 cm^{-2} and in UID2 was 10^5 cm^{-2}. Optical microscopy was performed to characterize the surface for macro-scale defects. In UID1, terraces were detected and the calculated density was approximately 10^7 cm^{-2}. However, in UID2, the terraces could not be observed most likely due to the difference in optical contrast resulting from the deposition of the Ti on the backside of the wafer. Generally, the variations in the wafers were understood to be normal fluctuations from the manufacturer.

Structural and optical characterization was performed in UID1 and UID2. X-ray characterization showed high threading dislocation densities in UID1. The screw dislocation density of (002) reflection was about 10^8 cm^{-2}, whereas, the mixed dislocation density of (102) reflection was 10^{10} cm^{-2}. The screw and mixed dislocation density in UID2 were 10^8 and 10^9 cm^{-2}, respectively. CL measurements were done to illustrate the optical quality of UID1. The measurements were at low temperature. The measurements were applied in several places, and they showed that the GaN bandgap energy is about 3.4 eV as expected. Similarly, transmission measurements were performed on UID2 at room temperature to demonstrate the optical quality and the bandgap energy was again found to be approximately 3.39 eV as expected.

The same morphology characterization was performed on SI1 and SI2. AFM measurements showed that the substrates suffered from hexagonal hillocks with a density around 10^5 cm^{-2} in both semi-insulating substrates. No V-shape pits were observed in SI1 and SI2. There were some bumps that could be associated with, and extended from, the hexagonal hillocks. Although there were no observed V-shape pits, SEM and optical microscope characterizations exhibited much larger macro-scale pits with areal densities of about 10^2 cm^{-2}. Those macro-scale pits were about 300 μm in size.

The structural and optical characterizations were performed in SI1 and SI2. X-ray

diffraction results were analyzed in order to characterize the screw and mixed dislocation densities for the SI1 and SI2 substrates. X-ray characterizations showed high threading dislocation densities in SI1. The screw dislocation density of (002) reflection was about 10^8 cm^{-2}, while the mixed dislocation density of (102) reflection was 10^9 cm^{-2}. Similarly, the screw and mixed dislocation densities in SI2 were 10^8 and 10^9 cm^{-2}, respectively. These correlated well with the specifications from the manufacturer. CL measurements were performed on SI1. The measurements were at low temperature and were applied inside and outside of the large pits, and again confirmed the GaN bandgap energy to be about 3.4 eV. In CL measurements, three luminescent peaks were observed in addition to the near band edge emission, which were the violet, blue, and yellow band luminescence. These peaks were related to defects in the structure such as dislocations, vacancies, and point defects. In contrast, optical transmission measurements were performed on SI2 at room temperature to demonstrate the optical quality of the bandgap transition at approximately 3.39 eV.

In order to understand how these defects affect the subsequent growth, a 1 μm GaN layer was grown on the UID1 substrate. Mapping the sample using AFM characterization was done to study the defects on the surface. There were four types of defect which were detected. These were small pits, distorted pits, line, and edges. The small pit density and distorted pit density were 10^7 and 10^8 cm^{-2}, respectively. Furthermore, the total length of the lines was 25.43 μm. TEM measurements were performed to examine the structure defects.

GaN layer with thickness 1 μm was grown on SI1 substrate. AFM images exhibited some defects. The sample suffered from a high number of micro-scale pit density, macro-scale pits, and hillocks. The micro-scale pit density was approximately 10^8 cm^{-2}.

In future work, is that the TEM characterization should be done on SI1 to study the

structure defects and understand the defects that are related to the substrate. Photoluminescence should also be applied to UID1, UID2, SI1, and SI2 to compare the results with CL and transmission measurements and characterize the optical properties of those substrates and the subsequent growth. Ultimately, this work will assist in the development of future high quality growth recipes for GaN and other III-nitride materials on these HVPE substrates.

References

[1] Engneering Faculty website. [Online]. Available: http://faculty.engineering.asu.edu/zhao/. [Accessed: 12-Apr-2019].

[2] Tian Y, Shao Y, Wu Y, Hao X, Zhang L, Dai Y and Huo Q 2015 Direct growth of freestanding GaN on C-face SiC by HVPE *Sci. Rep.* **5** 1–8.

[3] Paskova T, Hanser D A and Evans K R 2010 GaN substrates for III-nitride devices *Proc. IEEE* **98** 1324–38.

[4] Beltz G E, Robertson C A, Romanov A E, Speck J S, Foronda H M and Young E C 2016 Curvature and bow of bulk GaN substrates *J. Appl. Phys.* **120** 035104.

[5] Motoki K 2010 Development of gallium nitride substrates *SEI Tech. Rev.* 28–35.

[6] Kukushkin, S & Osipov, Andrey & Bessolov, V & K Medvedev, B & K Nevolin, V & A Tcarik, K. (2008). Substrates for epitaxy of gallium nitride: New materials and techniques. Reviews on Advanced Materials Science. 17.

[7] Aunsborg T and Hjelmgart R. *Characterization of GaN thin films and growth by plasma-assisted molecular beam epitaxy.* MS Thesis. Aalborg University, 2016. p 31-39. Available: https://projekter.aau.dk/projekter/en/studentthesis/characterization-of-gan-thin-films-and-growth-by-plasmaassisted-molecular-beam-epitaxy(ad4cd2a3-31c4-4c93-a977-07617cabf7f3).html. [Accessed: 2-Mar-2019].

[8] Ryou J-H and Lee W 2018 GaN on sapphire substrates for visible light-emitting diodes *Nitride Semicond. Light. Diodes* 43–78.

[9] Litwin-Staszewska E, Piotrzkowski R, Bockowski M, Lucznik B, Amilusik M, Sochacki T, Iwinska M and Fijalkowski M 2017 (Invited) Growth and Characterization of Bulk HVPE-GaN – Pathway to Highly Conductive and Semi-Insulating GaN Substrates *ECS Trans.* **80** 991–1003.

[10] Nakamura S 1998 The Roles of Structural Imperfections in InGaN-Based Blue Light-Emitting Diodes and Laser Diodes *Science (80-.).* **281** 956–61.

[11] Moustakas T D and Pankove J I 1997 *Gallium nitride (GaN) I* (Academic Press). 315-400.

[12] Jang L-W, Jeon D-W, Polyakov A Y, Govorkov A V, Sokolov V N, Smirnov N B, Cho H-S, Yun J-H, Shcherbatchev K D, Baek J-H and Lee I-H 2014 Electrical and structural properties of GaN films and GaN/InGaN light-emitting diodes grown on porous GaN templates fabricated by combined electrochemical and photoelectrochemical etching *J. Alloys Compd.* **589** 507–12.

[13] Qin H, Luan X, Feng C, Yang D and Zhang G 2017 Mechanical, thermodynamic and electronic properties of wurtzite and zinc-blende GaN crystals *Materials (Basel).* **10** 1–15.

[14] Pugh K S, Dugdale D J, Brand S, and Abram, R A. (1999). Electronic Structure Calculations on Nitride Semiconductors. Semiconductor Science and Technology. 14. 23. 10.1088/0268-1242/14/1/003.

[15] Chen Jr-Tai, MOCVD growth of GaN-based high electron mobility transistor structures, PhD thesis. Linköping University, 2015. 5-11.

[16] Vitanov S, Palankovski V, Maroldt S, Quay R, Murad S, Rodle T and Selberherr S 2012 Physics-Based Modeling of GaN HEMTs *IEEE Trans. Electron Devices* **59** 685–93.

[17] Polyakov A Y, Smirnov N B, Govorkov A V., Dang G, Zhang A P, Ren F, Cao X A, Pearton S J and Wilson R G 2000 Electrical properties and defect states in undoped high-resistivity GaN films used in high-power rectifiers *J. Vac. Sci. Technol. B Microelectron. Nanom. Struct.* **18** 1237.

[18] Oh D-C 2009 Electrical Properties of GaN and ZnO (Springer, Berlin, Heidelberg) pp 355–414.

[19] Yan F. K., Low L. L., Oh S. A., Hasan Z., "Gallium Nitride: An Overview of Structural Defects," in *Optoelectronics Materials and Techniques*, Predeep P. ed. (InTech, Shanghai, China, 2011).

[20] Weyher J L, Kamler G, Nowak G, Borysiuk J, Lucznik B, Krysko M, Grzegory I and Porowski S 2005 Defects in GaN single crystals and homoepitaxial structures *J. Cryst. Growth* **281** 135–42.

[21] Moram M A and Vickers M E 2009 X-ray diffraction of III-nitrides *Reports Prog. Phys.* **72** 17-21.

[22] Kaganer V M, Brandt O, Trampert A and Ploog K H 2005 X-ray diffraction peak profiles from threading dislocations in GaN epitaxial films *Phys. Rev. B - Condens. Matter Mater. Phys.* **72** 1-3.

[23] Anon Crystal Defects, Line Defects, Planar Defects | Chemistry@TutorVista.com. [Online]. Available: https://chemistry.tutorvista.com/inorganic-chemistry/crystal-defects.html. [Accessed: 4-Mar-2019]

[24] Anon material science - What is the edge component and screw component of a Burgers vector? - Physics Stack Exchange. [Online]. Available: https://physics.stackexchange.com/questions/273453/what-is-the-edge-component-and-screw-component-of-a-burgers-vector. [Accessed: 5-Mar-2019]

[25] Keeping S 2013 Material and Manufacturing Improvements | DigiKey. [Online].

Available: https://www.digikey.com/en/articles/techzone/2013/jan/material-and-manufacturing-improvements-enhance-led-efficiency. [Accessed: 2-Feb-2019].

[26] Tawfik W Z, Hyun G Y, Ryu S-W, Ha J S and Lee J K 2016 Piezoelectric field in highly stressed GaN-based LED on Si (1 1 1) substrate *Opt. Mater. (Amst).* **55** 17–21.

[27] P. Visconti, K.M. Jones, M.A. Reshchikov, R. Cingolani, H. Morkoc, R. Molnar, Investigation of defects in GaN by photo-electronchemical and hot wet etching, Appl. Phys. Lett. **77** (2000) 3532.

[28] Keller S, Li H, Laurent M, Hu Y, Pfaff N, Lu J, Brown D F, Fichtenbaum N A, Speck J S, DenBaars S P and Mishra U K 2014 Recent progress in metal-organic chemical vapor deposition of N-polar group-III nitrides *Semicond. Sci. Technol.* **29** 113001.

[29] Oehler F, Zhu T, Rhode S, Kappers M J, Humphreys C J and Oliver R A 2013 Surface morphology of homoepitaxial c-plane GaN: Hillocks and ridges *J. Cryst. Growth* **383** 12–18.

[30] Hageman P R, Kirilyuk V, Corbeek W H M, Weyher J L, Lucznik B, Bockowski M, Porowski S and Müller S 2003 Thick GaN layers grown by hydride vapor-phase epitaxy: Hetero- versus homo-epitaxy *J. Cryst. Growth* **255** 241–9.

[31] Fujikura H, Konno T, Yoshida T and Horikiri F 2017 Hydride-vapor-phase epitaxial growth of highly pure GaN layers with smooth as-grown surfaces on freestanding GaN substrates *Jpn. J. Appl. Phys.* **56** 085503.

[32] Gott, A P. *Bulk gallium nitride overgrowth by hydride vapour phase epitaxy on compliant nano-column substrates*. Diss. University of Bath, 2007. 9-11. [Accessed: 4-May-2018].

[33] JPK Instruments AG 2005 The NanoWizard ® AFM Handbook 40.

[34] Anon Atomic Force Microscopy - Nanoscience Instruments. [Online]. Available: https://www.nanoscience.com/techniques/atomic-force-microscopy/. [Accessed: 6-Nov-2018].

[35] Anon 2018 An Introduction to Electron Microscopy - SEM. [Online]. Available: https://www.fei.com/introduction-to-electron-microscopy/sem/. [Accessed: 1-Dec-2018].

[36] Zhou W, Apkarian R, Wang Z L and Joy D 2007 Fundamentals of scanning electron microscopy (SEM) *Scanning Microsc. Nanotechnol. Tech. Appl.* 1–40.

[37] Anon Scanning Electron Microscopy - Nanoscience Instruments. [Online]. Available: https://www.nanoscience.com/techniques/scanning-electron-microscopy/. [Accessed: 9-Feb-2019].

[38] Chen X, Zheng B and Liu H 2011 Optical and digital microscopic imaging techniques and applications in pathology. *Anal. Cell. Pathol. (Amst).* **34** 5–18.

[39] Anon Optical Microscopes | Olympus IMS. [Online]. Available: https://www.olympus-ims.com/en/microscope/terms/feature10/. [Accessed: 15-Feb-2019].

[40] Rack P D *Optical Microscopy*. [Online]. Available: http://web.utk.edu/~prack/MSE%20300/Lightmicroscopyhandout.pdf. [Accessed: 14-Feb-2019].

[41] Hiscock I V. 2008 Laboratory Manual *Am. J. Public Health* **16** 1134–1136.

[42] Anon *X-ray Diffraction (XRD) • 1.0 What is X-ray Diffraction • 2.0 Basics of Crystallography • 3.0 Production of X-rays • 4.0 Applications of XRD • 5.0 Instrumental Sources of Error • 6.0 Conclusions*. [Online]. Available: http://web.pdx.edu/~pmoeck/phy381/Topic5a-XRD.pdf. [Accessed: 12-Feb-2019].

[43] Lee S R, West A M, Allerman A A, Waldrip K E, Follstaedt D M, Provencio P P, Koleske D D and Abernathy C R 2005 Effect of threading dislocations on the Bragg peakwidths of GaN, AlGaN, and AlN heterolayers *Appl. Phys. Lett.* **86** 241904.

[44] Nanyang Technological University 2013 Transmission Electron Microscope Training module *MyScope* 86. [Online]. Available: http://www.ammrf.org.au/myscope/pdfs/tem.pdf. [Accessed: 20-Feb-2019].

[45] Tang CY, Yang Z. Transmission electron microscopy (TEM). In: Hilal N, Ismail A, Matsuura T, Oatley-Redceiffe D, editors. Membrane characterization. Amesterdan: Elsevier; 2017. p. 145-59.

[46] Anon Cathodoluminescence – Semiconductor Spectroscopy and Devices. [Online]. Available: http://ssd.phys.strath.ac.uk/techniques/scanning-electron-microscopy/cathodoluminescence/. [Accessed: 25-Feb-2019].

[47] Anon 2018 Principles and Applications of SEM-CL (SEM-Cathodoluminescence). [Online]. Available: https://www.azom.com/article.aspx?ArticleID=16148. [Accessed: 20-Feb-2019].

[48] Gorman D 2001 Photoluminescence and Excitation Studies of Semiconductors School of Physical Sciences *Dissertation.* Dublin City University 2001. 14-20.

[49] Subash K. *The optical characterization of GaN, AlGaN and AlGaN-GaN-AlGaN quantum wells*. Diss. North Carolina State University 1993. 25-30.

[50] Henini, M. (Ed.). (2012). *Molecular beam epitaxy: from research to mass production*. Newnes. 228-230.

[51] Stehl, C., Fischer, M., Gsell, S., Berdermann, E., Rahman, M. S., Traeger, M., & Schreck, M. (2013). Efficiency of dislocation density reduction during heteroepitaxial growth of diamond for detector applications. *Applied Physics Letters, 103*(15), 151905.

[52] Oehler F, Sutherland D, Zhu T, Emery R, Badcock T J, Kappers M J, Humphreys C J, Dawson P and Oliver R A 2014 Evaluation of growth methods for the heteroepitaxy of non-polar (112¯0) GAN on sapphire by MOVPE *J. Cryst. Growth* **408** 32–41.

[53] Morkoc M A 2005 Luminescence properties of defects in GaN *J. Appl. Phys.* **97** 61301.

[54] Huang J, Xu K, Fan Y M, Wang J F, Zhang J C and Ren G Q 2014 Dislocation luminescence in GaN single crystals under nanoindentation *Nanoscale Res. Lett.* **9** 1–7.

[55] Reshchikov M A and Morkoç H 2005 Luminescence properties of defects in GaN *J. Appl. Phys.* **97** 061301.

[56] Reshchikov M A, Morkoç H, Park S S and Lee K Y 2002 Two charge states of dominant acceptor in unintentionally doped GaN: Evidence from photoluminescence study *Appl. Phys. Lett.* **81** 4970–2.

[57] Reshchikov M A, Zafar Iqbal M, Park S S, Lee K Y, Tsvetkov D, Dmitriev V and Morkoç H 2003 Persistent photoluminescence in high-purity GaN *Phys. B Condens. Matter* **340**–**342** 444–7.

[58] Monemar B 2001 Bound excitons in GaN *J. Phys. Condens. Matter* **13** 7011–26.

Appendix A: Description of Research for Popular Publication

Defect Characterization of HVPE GaN Substrates and GaN Growth

By: Alaa Kawagy

Scientists at the University of Arkansas are working to improve gallium nitride (GaN) materials and their applications. Alaa Kawagy is a graduate student that was studying and characterizing GaN substrates to understand the features in the structural and the micro-scale properties of the surface of the material. Before going deep in these features, questions as “what is GaN material”, “and what is it use for” should be answered.

GaN is a semiconductor material that has good properties that can help to improve electrical and optoelectrical devices. GaN materials are used in scientific and daily applications. For example, they are used in LED lights, semiconductor lasers, solar cells, sensors, and some medical applications. Since assistant professor Morgan Ware is interested in this material, he and his group are working in GaN applications and characterization. One of his students, Alaa Kawagy, was principally characterizing GaN templates. Alaa characterized the structural quality and the surface quality.

Alaa used several techniques to characterize the structural quality. She used the x-ray diffraction technique to learn about the quality of the template and determine if they have defects. She said GaN materials that she characterized suffered from high defect densities. These defects are screw dislocations which are similar to spiral stair cases in the crystal. In addition, edge dislocations were detected by x-ray diffraction, which are characterized by missing a “half-plane” of atoms in the crystal. Moreover, she used the optical transmission technique to study the optical properties. She said that the templates have good optical qualities since they demonstrate reasonable bandgap energy. Another technique that she used was cathodoluminescence which

characterizes the structural qualities and detects any defect in the structure. From these cathodoluminescence measurements, she found that some of templates suffered from defects such as missing atoms or dislocations in the structure. However, some of them seem to be good crystals and did not suffer from defects.

In addition, Alaa characterized the surface of these templates. She used atomic force microscopy, scanning electron microscopy, and optical microscopy. She used these techniques to see if the defects in the structure affect the surface. She said that the templates suffer from large defects in the surface. Some of these large defects come from the structural defects. They start from the structure and continue to the surface. They appear as small or large pits and as hillocks which look like bumps.

After a fresh layer of GaN was grown on some of these templates, Alaa characterized them again to see if the defects in the templates would affect the subsequent growth. She said some of the defects propagated to the new layer. The defects that were detected in the new layer were small and large pits and hillocks. Since she characterized the whole surface, she said that the defects were spread randomly. However, the right side from the templates had less defects, so it was the best place to fabricate a device.

Appendix B: Executive Summary of Newly Created Intellectual Property

Determining the defects in Hydride Vaper Phase Epitaxy GaN on sapphire substrates helps to improve the subsequent growth by avoiding the areas that have high defect density. The following list of new intellectual property items were created in the course of this research project and should be considered from both a patent and commercialization perspective.

1- Characterizing the whole surface of 2-inch wafers to study the morphology and the distribution of the defects and determine the best area for growth.
2- Using several methods of morphology characterizations to prove that the selected area is good for growth and subsequent fabrication of devices.
3- Characterizing the structure of the substrates by using several methods to study the optical and material properties.
4- Comparing and connecting the morphology defects with some of the structure defects to understand the reasons behind the surface defects.
5- Studying the following growth morphology to compare with the substrate morphology.
6- Characterizing the structure of the following growth to see if the defects in the surface resulted from the substrates by using transmission electron microscopy.

Appendix C: Potential Patent and Commercialization Aspects of listed Intellectual Property Items

C.1 Patentability of Intellectual Property

The characterizations of HVPE GaN on sapphire substrates are considered as a fundamental information for the following growth and improving the devices efficiencies by using the clearest area from defects. The items listed were considered first from the perspective of whether or not the item could be patented.

1- The morphology characterizations of HVPE GaN on sapphire substrates have been reported in many prior publications. Therefore, the morphology characterizations cannot be patented

2- The surface characterizations of HVPE GaN on sapphire substrates have been reported in many prior publications, so they cannot be patented.

3- The mapping of the whole 2-inch wafers to determine the defects and find the appropriate area for growth and the devices have been reported. Therefore, it cannot be patented.

C.2 Commercialization Prospects

The characterization of HVPE GaN on sapphire substrates presented in this thesis was to discover the defects and how these defecs affect the GaN electrical, optical, and material properties. In addition, the characterization presents more information about the variation of defects in the same sample and how they affect the subsequent growth. Even though the characterization methods cannot be patented, the methods can help companies improve the quality of their commercial wafers.

C.3 Possible Prior Disclosure of IP

There was no prior disclosure of IP.

Appendix D: Broader Impact of Research

D.1 Applicability of Research Methods to Other Problems

The characterization techniques such as x-ray, AFM, SEM, optical microscope used in this thesis can be applied on most of the semiconductor materials to study their structural properties and their morphology. Also, these characterization methods can help to provide some optical properties for semiconductor materials using CL and optical transmission. Furthermore, the TEM can be used to study the subsequent growth of the semiconductor substrates.

D.2 Impact of Research Results on U.S. and Global Society

The results of these characterizations beside the GaN properties can lead to improvements in the efficiencies of many electronic and optoelectronic devices such as solar cells, lasers, sensors, and LEDs. By building devices in areas with less defects, the performance of the devices will be improved. Such devices also are cost-effective because they have long lifetime and low power consumption which will be good for the society.

D.3 Impact of Research Results on the Environment

GaN is a promising material that is used in several useful applications which can positively impact the environment. For example, GaN is used in light emitting diodes which are energy efficient and cost effective and have long life time span. The second example is solar cells. The use of solar cells to generate electricity will lead to reduce the cost of the electricity. Also, solar cells provide pollution-free power sources. Solar cells are renewable energy and it does not need fuel, coal or gas to generate power. Which means it is a clean source of energy for the environment. Moreover, sensors based GaN and III-nitride can be promising for transportation. It can be used in electric vehicles which will provide a cleaner environment.

Appendix E: Microsoft Project for MS MicroEP Degree Plan

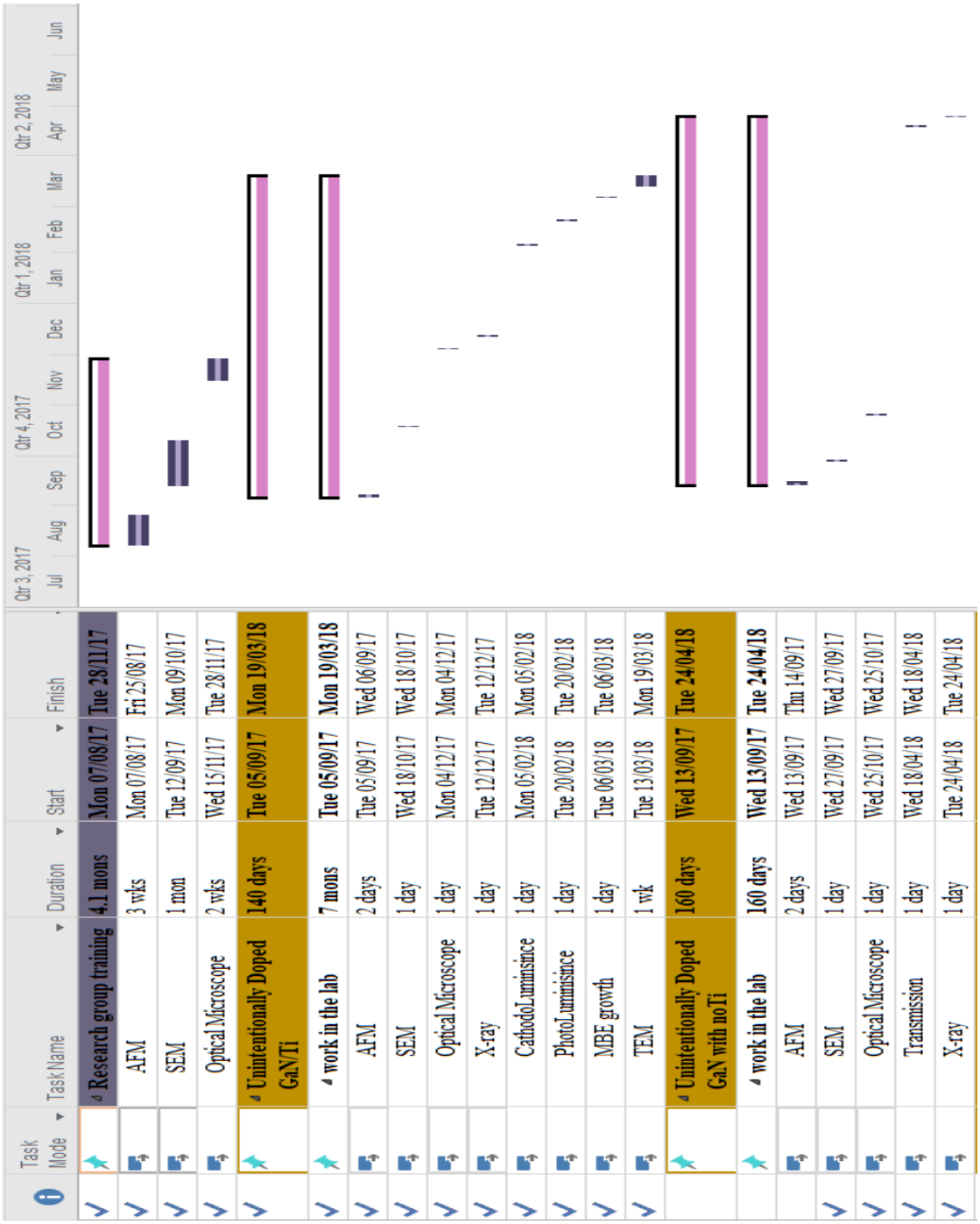

Task Mode	Task Name	Duration	Start	Finish
	Research group training	4.1 mons	Mon 07/08/17	Tue 28/11/17
	AFM	3 wks	Mon 07/08/17	Fri 25/08/17
	SEM	1 mon	Tue 12/09/17	Mon 09/10/17
	Optical Microscope	2 wks	Wed 15/11/17	Tue 28/11/17
	Unintentionally Doped GaNTi	140 days	Tue 05/09/17	Mon 19/03/18
	work in the lab	7 mons	Tue 05/09/17	Mon 19/03/18
	AFM	2 days	Tue 05/09/17	Wed 06/09/17
	SEM	1 day	Wed 18/10/17	Wed 18/10/17
	Optical Microscope	1 day	Mon 04/12/17	Mon 04/12/17
	X-ray	1 day	Tue 12/12/17	Tue 12/12/17
	CathodoLuminsince	1 day	Mon 05/02/18	Mon 05/02/18
	PhotoLuminisince	1 day	Tue 20/02/18	Tue 20/02/18
	MBE growth	1 day	Tue 06/03/18	Tue 06/03/18
	TEM	1 wk	Tue 13/03/18	Mon 19/03/18
	Unintentionally Doped GaN with noTi	160 days	Wed 13/09/17	Tue 24/04/18
	work in the lab	160 days	Wed 13/09/17	Tue 24/04/18
	AFM	2 days	Wed 13/09/17	Thu 14/09/17
	SEM	1 day	Wed 27/09/17	Wed 27/09/17
	Optical Microscope	1 day	Wed 25/10/17	Wed 25/10/17
	Transmission	1 day	Wed 18/04/18	Wed 18/04/18
	X-ray	1 day	Tue 24/04/18	Tue 24/04/18

Task Mode	Task Name	Duration	Start	Finish
	Classes	30.25 mons?	Mon 22/08/16	Fri 14/12/18
	Fall 2016	4.15 mons	Tue 23/08/16	Thu 15/12/16
	Semiconductor Device	4 mons	Tue 23/08/16	Mon 12/12/16
	TEM Class	4 mons	Tue 23/08/16	Mon 12/12/16
	STEM Field writing	4 mons	Tue 23/08/16	Mon 12/12/16
	Infrastructure Management	4 mons	Tue 23/08/16	Mon 12/12/16
	Spring 2017	4.15 mons	Tue 17/01/17	Thu 11/05/17
	Laser Physics	4 mons	Fri 20/01/17	Thu 11/05/17
	Nanofabrication Lab	4 mons	Fri 20/01/17	Thu 11/05/17
	Personnal Management	4 mons	Fri 20/01/17	Thu 11/05/17
	Fall 2017	4.15 mons	Tue 22/08/17	Thu 14/12/17
	IC Fab Technology	4 mons	Fri 25/08/17	Thu 14/12/17
	Microfabrication Lab	4 mons	Fri 25/08/17	Thu 14/12/17
	Management and Leadership	4 mons	Fri 25/08/17	Thu 14/12/17
	Spring 2018	4.15 mons	Tue 16/01/18	Thu 10/05/18
	commercialization of Research	4.15 mons	Tue 16/01/18	Thu 10/05/18
	Adv. Management and Leadership	4.15 mons	Tue 16/01/18	Thu 10/05/18
	Summer 2018	2.45 mons	Thu 31/05/18	Tue 07/08/18
	Engineering and Science Ethics	2.45 mons	Thu 31/05/18	Tue 07/08/18
	Fall 2018	4.15 mons?	Wed 22/08/18	Fri 14/12/18
	Electronic Materials	4.15 mons?	Wed 22/08/18	Fri 14/12/18

Task Mode	Task Name	Duration	Start	Finish
	Semi-Insulating GaN/Ti	**55 days**	**Mon 13/08/18**	**Fri 26/10/18**
	work in the lab	**55 days**	**Mon 13/08/18**	**Fri 26/10/18**
	AFM	3 days	Mon 13/08/18	Wed 15/08/18
	SEM	1 day	Tue 28/08/18	Tue 28/08/18
	Optical Microscope	1 day	Mon 03/09/18	Mon 03/09/18
	X-ray	1 day	Tue 11/09/18	Tue 11/09/18
	CathodoLuminisince	1 day	Thu 27/09/18	Thu 27/09/18
	PhotoLuminsince	1 day	Mon 01/10/18	Mon 01/10/18
	MBE growth	1 day	Tue 09/10/18	Tue 09/10/18
	TEM	1 wk	Mon 22/10/18	Fri 26/10/18
	Semi-Insulating GaN with no Ti	**77 days**	**Mon 03/12/18**	**Tue 19/03/19**
	work in the lab	**77 days**	**Mon 03/12/18**	**Tue 19/03/19**
	AFM	3 wks	Mon 03/12/18	Fri 21/12/18
	SEM	1 day	Wed 20/02/19	Wed 20/02/19
	Transmission	1 day	Mon 04/03/19	Mon 04/03/19
	x-ray	1 day	Tue 19/03/19	Tue 19/03/19
	Thesis	**111 days**	**Sat 01/12/18**	**Fri 03/05/19**
	write thesis	100 days	Sat 01/12/18	Fri 19/04/19
	edit	4 wks	Fri 01/03/19	Thu 28/03/19
	review by the advisor	4 wks	Fri 01/03/19	Thu 28/03/19
	Thesis Defense Presentation Construction	2 wks	Tue 19/03/19	Mon 01/04/19
	Final Thesis Revisions	2 wks	Thu 28/03/19	Wed 10/04/19
	Public Defense	1 day	Tue 16/04/19	Tue 16/04/19
	Committee Defense	**1 day**	**Tue 23/04/19**	**Tue 23/04/19**
	Graduation	**1 day**	**Fri 03/05/19**	**Fri 03/05/19**

Appendix F: Identification of All Software Used in Research and Thesis Generation

Computer #1:

Model Number: Inspiron 5459

Serial Number: HY2JGC2

Location: Home

Owner: Alaa Kawagy

Software #1:

Name: Microsoft Office 2016

Purchased by: University of Arkansas Site License

Software #2:

Name: Microsoft Project 2010

Purchased by: MSDN Academy Alliance through Engineering

Software #3:

Name: Origin 2018

Purchased by: Alaa Kawagy

Software #4:

Name: Nanoscope Analysis 1.6

Purchased by: Free

Software #5:

Name: ImageJ

Purchased by: Free

Computer #2:

Model Number: Latitude E5536 non-vPro

Serial Number: C7YFX1

Location: NANO 129

Owner: Dr. Greg Salamo

Software #3:

Name: Nanoscope Analysis 1.5

License: Free

Computer #3:

Model Number: MacBook Pro9,1

Serial Number: C02JX41FDV33

Location: Home

Owner: Alaa Kawagy

Software #1:

Name: Microsoft Office 2016

Purchased by: University of Arkansas Site License

Software #2:

Name: Nanoscope Analysis 1.5

Purchased by: Free

Software #5:

Name: ImageJ

Purchased by: Free

Appendix H: All Publications Published, Submitted, and Planned

No publications have been published or submitted for this work.